University of Windsor
Scholarship at UWindsor

Electronic Theses and Dissertations | Theses, Dissertations, and Major Papers

10-30-2020

# Design and Modeling of Piezoelectric Micromachined Ultrasonic Transducer (PMUT) using a Multi-User MEMS Process for Medical Imaging

Jenitha Antony Balasingam
*University of Windsor*

Follow this and additional works at: https://scholar.uwindsor.ca/etd

Recommended Citation
Antony Balasingam, Jenitha, "Design and Modeling of Piezoelectric Micromachined Ultrasonic Transducer (PMUT) using a Multi-User MEMS Process for Medical Imaging" (2020). *Electronic Theses and Dissertations*. 8433.
https://scholar.uwindsor.ca/etd/8433

This online database contains the full-text of PhD dissertations and Masters' theses of University of Windsor students from 1954 forward. These documents are made available for personal study and research purposes only, in accordance with the Canadian Copyright Act and the Creative Commons license—CC BY-NC-ND (Attribution, Non-Commercial, No Derivative Works). Under this license, works must always be attributed to the copyright holder (original author), cannot be used for any commercial purposes, and may not be altered. Any other use would require the permission of the copyright holder. Students may inquire about withdrawing their dissertation and/or thesis from this database. For additional inquiries, please contact the repository administrator via email (scholarship@uwindsor.ca) or by telephone at 519-253-3000ext. 3208.

www.manaraa.com

# Design and Modeling of Piezoelectric Micromachined Ultrasonic Transducer (PMUT) using a Multi-User MEMS Process for Medical Imaging

By

**Jenitha Antony Balasingam**

A Thesis
Submitted to the Faculty of Graduate Studies
through the Department of Electrical and Computer Engineering
in Partial Fulfillment of the Requirements for
the Degree of Master of Applied Science
at the University of Windsor

Windsor, Ontario, Canada

2020

© 2020 Jenitha Antony Balasingam

www.manaraa.com

**Design and Modeling of Piezoelectric Micromachined Ultrasonic Transducer (PMUT) using a Multi-User MEMS Process for Medical Imaging**

by

**Jenitha Antony Balasingam**

APPROVED BY:

_____

J. Johrendt

Department of Mechanical, Automotive & Materials Engineering

_____

S. Alirezaee

Department of Electrical & Computer Engineering

_____

A. Emadi, Advisor

Department of Electrical & Computer Engineering

July 30, 2020

www.manaraa.com

# DECLARATION OF CO-AUTHORSHIP / PREVIOUS PUBLICATION

I. Co-Authorship

I hereby declare that this thesis incorporates material that is result of joint research, as follows:

This thesis includes outcome of publications which also have co-authors who are/were students or post-doctoral fellow supervised by Dr. Arezoo Emadi. The co-authors are Haleh Nazemi, Siddharth Swaminathan, Dr. Ken Ambrose, Muhammad Umair Nathani, Tara Ahmadi and Yameema Babu Lopez.

Chapter 4 and 5 of this thesis includes a paper submitted to IEEE IUS 2020 Conference for publication. The paper was co-authored with Siddharth Swaminathan and Dr. Arezoo Emadi. Chapter 6 of this thesis includes a paper published in MDPI Journal of Sensors. The paper was co-authored with Haleh Nazemi, Siddharth Swaminathan, Dr. Ken Ambrose, Muhammad Umair Nathani, Tara Ahmadi, Yameema Babu Lopez and Dr. Arezoo Emadi. In all cases, the key ideas, primary contributions, experimental designs, data analyses and writing were performed by the author and the contribution of co-authors was primarily through the provision of assistance contributed to the statistical analyses and graphing results and provided feedback in manuscript preparation and refinement of ideas.

I am aware of the University of Windsor Senate Policy on Authorship and I certify that I have properly acknowledged the contribution of other researchers to my thesis, and have obtained written permission from each of the co-author(s) to include the above material(s) in my thesis.

I certify that, with the above qualification, this thesis, and the research to which it refers, is the product of my own work.

II. Previous Publication

This thesis includes 2 original papers that have been previously published/submitted for publication in peer reviewed journals, as follows:



www.manaraa.com

| Thesis Chapter | Publication Title | Publication status |
|---|---|---|
| Chapter 4, 5 & 6 | **J. Antony Balasingam**, S. Swaminathan and A. Emadi, "A Low-Frequency Piezoelectric Micromachined Ultrasonic Transducer based on Multi-User MEMS Process with Enhanced Output**"** *IEEE IUS Sensors, 2020* | Accepted |
| Chapter 6 | H. Nazemi, **J. Antony Balasingam**, S. Swaminathan, K. Ambrose, M.U. Nathani, T. Ahmadi, Y. Babu Lopez and A. Emadi, "Mass Sensors Based on Capacitive and Piezoelectric Micromachined Ultrasonic Transducers-CMUT and PMUT" *Sensors, 2019* | Published |

I certify that I have obtained a written permission from the copyright owner(s) to include the above published material(s) in my thesis. I certify that the above material describes work completed during my registration as a graduate student at the University of Windsor.

I declare that, to the best of my knowledge, my thesis does not infringe upon anyone's copyright nor violate any proprietary rights and that any ideas, techniques, quotations, or any other material from the work of other people included in my thesis, published or otherwise, are fully acknowledged in accordance with the standard referencing practices. Furthermore, to the extent that I have included copyrighted material that surpasses the bounds of fair dealing within the meaning of the Canada Copyright Act, I certify that I have obtained a written permission from the copyright owner(s) to include such material(s) in my thesis.

I declare that this is a true copy of my thesis, including any final revisions, as approved by my thesis committee and the Graduate Studies office, and that this thesis has not been submitted for a higher degree to any other University or Institution.



www.manaraa.com

# ABSTRACT

According to the Canadian Cancer Society, 2020, "1 in 8 women will be affected by breast cancer and 1 in 33 will die from it." There has been decline in the breast cancer causalities due to the early detection using advanced imaging technologies. This signifies the importance of early detection of breast cancer that increases the survival rate and treatment options for the patients. One of the platforms which is aiding the early detection is Microelectromechanical Systems (MEMS)-base imaging system. In this thesis, a Piezoelectric Micromachined Ultrasonic Transducer (PMUT) is proposed to work at lower frequency ranges for higher penetration aiding imaging applications while operating at lower voltage. In this work, a comprehensive study based on the Multi-User MEMS Process (MUMPs) has been conducted to investigate the effect of critical design parameters on the output performance. Three sets of PMUTs are fabricated based on the investigated parameters. The resonant frequency and acoustic output pressure of these fabricated devices are evaluated and compared based on their respective areas of piezo layer using COMSOL Multiphysics. The resonant frequency of the fabricated PMUT ranges from 0.5 MHz to 2 MHz. Keysight Impedance Analyzer E4990A has been utilized for the electrical characterization of the fabricated PMUT devices to determine their respective resonant frequencies and validate the COMSOL simulation results. It is shown that the fabricated individual circular PMUT achieves a high acoustic output pressure of 39 kPa at 1.3 MHz and the rectangular PMUT provides 4.7 kPa of acoustic pressure at 1.4 MHz. The results indicate that the proposed PMUT design can deliver acoustic pressure at a lower frequency range to increase the penetration depth.



www.manaraa.com

# DEDICATION

*To all the women in the world.*



www.manaraa.com

# ACKNOWLEDGEMENTS

Every achiever is inspired by a great mentor. First and foremost, I would like to thank my mentor Dr. Arezoo Emadi who guided me through various challenges. She has always provided me with the resources that were required for my research. I am forever indebted to you for giving me an opportunity to inspire many people and show them the value of education. Thank you for giving me those three options which changed my life for the better and also for not giving up on me.

I wish to express my sincere gratitude to my thesis committee members Dr. Jennifer Johrendt and Dr. Shahpour Alirezaee for their constructive feedback and valuable suggestions. I would like to thank them for their time and support.

There are friends, there is family and then there are friends that become family. I would like to thank Jaewoo Park, Matthew Santos, Niwit Aryal, Jay Nagarajan, Haleh Nazemi, Siddhu, Muhammad Umair Nathani and all the e-Minds family for accepting me as one of them and sharing my victories and hardships. Your constant support and encouraging words have always uplifted me.

My greatest thanks to my Amma and Appa for the wings you have given me. Without their blessings and sacrifices, I would not have made it to this stage. And my brother Jeffy kuti whose love has always defied the distance of a thousand miles between us. You have always been and will be close to me. I would like to include my Canadian family Dany, Thagapa & The Dunns' for being my backbone in this rollercoaster ride.

Last but not least, I would like to thank the almighty God for being the tiny voice of support in me, when the whole world seemed too loud.



www.manaraa.com

# TABLE OF CONTENTS





www.manaraa.com

www.manaraa.com

www.manaraa.com

# LIST OF TABLES





www.manaraa.com

# LIST OF FIGURES





www.manaraa.com

www.manaraa.com

www.manaraa.com

www.manaraa.com

www.manaraa.com

www.manaraa.com

# Chapter 1

# Introduction

*"It always seems impossible until it's done"*

*- Nelson Mandela*

## 1.1 Motivation

Breast cancer continues to be a pressing health issue for women of all ages. It is the second prominent death-causing disease for Canadian women. According to the Canadian Cancer Society, 2020, "1 in 8 women will be affected by breast cancer and 1 in 33 will die from it." As per the 2020 survey, it is assessed that 27,000 women will be identified with breast cancer and 5100 women will die from it. Uncommonly, 240 men are predicted to be diagnosed with breast cancer and 55 will die from it. The alarming figures in the statistics exhibit an upward trend for 50 years. In Canada, the number of cases significantly increased between 1984 and 1991 and elevated during 1986 [1]. However, there can be a decline in the mortality rate if early detection tools and advanced imaging technologies are employed. This implies the importance of early detection of breast cancer as it increases the survival rate and treatment options for the patients.

The breast is primarily made of the fat tissues. Hence, a sensitive imaging device is required to differentiate the cancerous tissues from the fat tissues of the breast. Ultrasound, a non-invasive method to identify the tumours, can be potentially more sensitive than X-ray mammography in differentiating the tissues [2]. Considering these facts, an advanced detecting device, when miniaturized using the MEMS technology, can not only facilitate the early detection but also increase the feasibility of developing a



www.manaraa.com

transportable device. This MEMS-based ultrasound would shift the point of care for breast cancer testing from clinics to home in future. A MEMS-based ultrasound transducer, one of the non-invasive detection methods, is an active topic for researchers. Based on the actuating mechanism, it is categorized into Piezoelectric Micromachined Ultrasonic Transducer (PMUT) and Capacitive Micromachined Ultrasonic Transducer (CMUT). The major characteristics for a transducer are frequency bandwidth, electromechanical coupling, quality factor, acoustic impedance match between two media, power consumption, and more importantly acoustic power generation ability.

Unlike bulk transducers, PMUT can be easily batch fabricated, is cost-effective and offers integration with electronic circuits such as portable devices. The existing conventional ultrasound transducers and parallel PMUT designs are studied and analyzed. The investigation shows that the conventional ultrasound transducer facing a major issue in differentiating the target or infected area due to the problems such as narrow bandwidth and high acoustic impedance between the media [3]. However, PMUT provides a high capacitance, low polarization voltage due to the piezoelectric property and compatible for micromachining processes which reduce the bulkiness. Therefore, PMUT is considered to be a potential candidate for early breast cancer detection as well as the medical imaging field.

## 1.2 Thesis Contribution

In this thesis, PMUT transducers are designed, analyzed, developed, and evaluated focusing mainly on early breast cancer detection in the domain of medical imaging. The main objective of the thesis is to develop a PMUT that operates at a lower frequency range capable of generating acoustic output pressure for ultrasound imaging. The lower end of



www.manaraa.com

the frequency range is targeted as they have better penetration through the medium with less attenuation. To design this PMUT, the principle of operation is studied and analyzed to investigate the effect of critical parameters on resonant frequency and acoustic output pressure with the respective equations. The effect of piezoelectricity is also studied for the proposed circular, square and rectangular PMUT designs. An equivalent circuit model is analyzed for a better understanding of electromechanical coupling in a structure.

A layer by layer analyses along with analytical modelling has been done for the proposed PMUT structure. The analyses show that the governing equations cannot hold for a multilayered complex structure of PMUT. Therefore, the factors causing the deviation of the calculated values from the simulated values are studied and evaluated. The COMSOL Multiphysics software is used to investigate the optimal value for the critical parameters such as radius, thickness and material of a layer, applied AC voltage and different test medium. The appropriate boundary conditions are applied to the structure to run both the electrical and acoustic analyses. The determination of resonant frequency is carried out through this finite element analyses method. This process is done to design a lower frequency PMUT by varying the critical parameters affecting the resonant frequency. Then, the PMUT is operated at their respective resonant frequency of the proposed designs, the acoustic output is analyzed to deliver the output pressure. Different medium and critical parameters have been studied and evaluated in the acoustic analyses of the PMUT.

The proposed designs of the PMUT are fabricated using the PiezoMUMPs fabrication technology and packaged using CPGA209A. The PMUT chip layout is designed using the MEMS Pro software. The fabricated PMUT chip – IMPWR001 is then electrically characterized and measured using the impedance analyzer. Comparison



www.manaraa.com

between the simulated resonant frequency from COMSOL and the measured values from the impedance analyzer agrees well. Therefore, a low frequency PMUT is designed to deliver the acoustic output pressure.

## 1.3 Thesis Outline

In Chapter 2, various medical imaging technologies such as Radiography, Tomography, Nuclear Medicine, Magnetic Resonance Imaging (MRI) and Ultrasound along with the principles of operation are reviewed. Moreover, the capacitive micromachined ultrasound transducer (CMUT), as well as PMUT, are studied.

In Chapter 3, a comprehensive study has been done on the principle of operation of PMUT. The piezoelectric effect along with the equivalent circuit model is studied. The effect of critical parameters such as radius, thickness and geometry on resonant frequency and acoustic output pressure are studied and analyzed.

Chapter 4 includes the layer by layer electrical analyses of the PMUT structure using the COMSOL Multiphysics software. Appropriate boundary conditions along with the critical parameters analyses have been done for each layer. Moreover, the analytical modelling has been done and the calculated values are compared with the simulated values.

In Chapter 5, the critical parameters are analyzed for the acoustic simulations. The acoustic output pressure is determined for various radii, thickness and medium for the proposed designs.

Chapter 6 outlines the PiezoMUMPs fabrication technique which is selected to fabricate the proposed PMUT designs. The fabrication steps of the proposed PMUT is discussed in detail. Furthermore, the proposed PMUT design layout is discussed along with



www.manaraa.com

the electrical characterization of the PMUT chip – IMPWR001. Then, the comparison of simulated data and the measured data has been done to determine the resonant frequency of the PMUT.

Finally, Chapter 7 provides the conclusion and the summary of the thesis and potential future works are further provided.



www.manaraa.com

# Chapter 2

# Medical Imaging Technologies

*"Indeed, we often mark our progress in science by improvements in imaging."*

*- Martin Chalfie*

## 2.1 Introduction

From unrefined to life-like images, one can trace the evolution of Medical Imaging. This involves not only the technology but also the minds who have changed concepts into medical marvels. The primordial medical diagnosis involves palpating, auscultation, percussion and specimen observation [4]. Over the centuries, the basic drawbacks of diagnostic methods caused a lack of reliability and precision. At the end of the 18th century, the world of medicine and science experienced an alteration with the discovery of invisible rays called X-rays by Wilhelm Conrad Rontgen [5]. The medical imaging became more quantitative and contributed towards the diagnosis of diseases. It met the need for treatment involving earlier detection, cost-effectiveness, reliability and less human intervention. The process of visualizing the inner organs demands a multitude of technologies. In this chapter, various medical technologies such as Radiography, Tomography, Magnetic Resonance Imaging (MRI), Nuclear Medicine and Ultrasound will be reviewed, discussed, and compared.



www.manaraa.com

## 2.2 Radiography

Without having to do surgery, X-rays help doctors observe the inner organs. X-rays are high-energy beams of electromagnetic radiation and are invisible to human eyes. When a high voltage is applied to accelerate the electrons in a vacuum tube consisting of a cathode and an anode, X-rays are generated. Their energy level ranges between 10eV to 100eV which facilitates the penetration through the tissue and air of the target object. But they are blocked when encountered by the materials of high density such as tumor, metal or bone [6] [7].

In order to get an image of the part or patient to be examined, the desired area is placed between the X-ray beam and a coated plate. The quality of the image is proportional to the density, geometry, distance and medium. The X-rays pass through the thinner materials and appears white whereas the denser materials appear as black or a shadow when the plate is processed. A qualified physician deciphers the processed photographic negative image for the patients. This entire process takes only a few minutes and based on the organ to be tested, the duration varies [8].

The main limitation of X-rays is radiation exposure. Prolonged exposure results in skin burn, radiation sickness, tissue damage and even cause defects in genes. Furthermore, the patients who have been implanted with monitoring devices like Pacemaker are prone to electrical disturbances due to the radiation. X-rays are highly inadvisable for pregnant women as the radiation will affect the fetus. Another significant drawback is the disability of the X-rays to process moving objects such as the heart. The movement of the target object compromises the resolution of the image. The aforementioned limitations of Radiography prompted the medical science to develop to a better imaging technique [9].



www.manaraa.com

## 2.3 Tomography

The limitation of radiography was overcome by an impressive computational speed and a high-power imaging technique called X-ray Computed Tomography also known as CT, CAT Scan (Computed Axial Tomography) scan or X-Ray CT scan [10]. The resultant image is a two-dimensional slice of a three-dimensional target object, called a Tomogram. In this process, the object or patient to be analyzed is placed between equipment with an X-ray source or generator and X-ray detector. This follows a simple principle of relative motion of X-ray source and detector in opposite directions which determines the focal point in the desired area and blurs out the remaining area. The tomogram is reconstructed using a mathematical algorithm [11]. The development of technology contributes to the advancements in this technique such as Spiral Scanning, Electron Beam CT, CT Fluoroscopy, and Multi-Slice Scanners. These processes address the major limitation such as the insufficient information about density distribution and depth of the layers in a structure [12].

This process of scanning is brief and inexpensive. However, radiation exposure is a common setback to both the conventional and advanced process of computed tomography. The three factors that determine radiation exposure are absorbed dose effective dose and collective dose. They are expressed in Computed Tomography Dose Index (CTDI) and Dose-Length Product (DLP). Based on these three factors, the exposure in CT ranges between 10-100 mGy (milliGray). This prolonged exposure to radiation might increase the risk of developing cancer. The size and design of the CT scanner also play a predominant role. Statistics of diagnostic radiology from hospitals indicates that CT



www.manaraa.com

contributes 75% radiation dosage. Limiting the examination time might solve the problem but in turn, it compromises the quality of the image or the tomogram [13].

## 2.4 Nuclear Medicine

The process of using the nuclear properties of radioactive materials such as Calcium-14, Carbon-15, in diagnosis and research is, Nuclear Medicine. This procedure is performed with other imaging techniques generally for detecting rather than curing the disease [14]. A prescribed amount of radioactive material is either injected, inhaled or ingested into the bloodstream followed by a waiting period. A window of thirty minutes is given for the material to concentrate on the body part to be diagnosed. Once the material starts disintegrating into the bloodstream, it emits electromagnetic radiation. Based on the nuclear properties of the material, the rate of decay varies. High-end detectors such as gamma cameras trace down the radiation. This machine is capable of converting the radiation into electrical signals which results in a black and white image and the diagnosed area in programmed colors. A nuclear medicine physician or radio pharmacist deciphers the processed image to patients. The radioactive material decays quickly and is passed out through body fluids [15]. The diagnostic procedure in nuclear medicine uses invasive methods for imaging which puts children and pregnant women at risk. Furthermore, this therapy is limited to diagnosing large tumors as they require a higher intake of radioactive material to detect smaller and deeper tumors. The accessibility to the machines and slower adaptation by clinicians to learn the technology makes it unattainable for impoverished countries. It covers only 10% to 20% of the targeted people as it is not affordable in most cases [16].



www.manaraa.com

## 2.5 Magnetic Resonance Imaging

The human body is mostly made of fat, proteins, minerals and water as shown in Table I [17]. Among these, water plays a significant role. The alignment of water molecules in tissue is controlled by the magnetic field created by the primary and secondary magnets. This facilitate the imaging mechanism of Magnetic Resonance Imaging (MRI). MRI relies on the magnetic characteristics of the water molecule to look deep into the body to give detailed images. The setup consists of a super conducting magnet (primary magnet), gradient coils (secondary magnet), transmitting and receiving radio frequency (RF) coils, RF detector and computer system. The three gradient coils (secondary magnet) attached to the primary magnet, gives the MRI to image in three axes [18].

***Table I*** *shows the percentage of water present in human body*

| Name of the Organs in human body | Amount of water present in each organ (%) |
|---|---|
| Brain and Heart | 73 |
| Lungs | 83 |
| Skin | 64 |
| Muscles and Kidneys | 79 |
| Bones | 31 |
| Liver | 71 |

Under normal conditions, water molecules move randomly. The primary magnet produces a magnetic field of strength 1.5 to 3T, which aligns the water molecules in the targeted area to a particular frequency. The majority of water molecules align in the direction of the primary magnetic field. RF coils are used to transmit the radio frequency and produce a secondary magnetic source which realigns the molecule. After a few seconds, the secondary source is switched off, which realigns the molecules again. This results in the



www.manaraa.com

frequency shift of the water molecules [19]. This change in frequency induces an electrical signal and it is received by the RF detector. Based on the type of tissue, resolution of the image varies accordingly. The generalization of the test results of the patients results in accuracy and questions the validity of the MRI [20]. The higher expense in conducting clinical study and intricacies in technical development slows down the process of implementation. Moreover, the strong magnetic field generated by MRI machines makes it hard for the patients with implanted devices as it creates a magnetic and electrical disturbance in their devices which may lead to fatal internal injuries [21] [22].

## 2.6 Ultrasound Imaging

Ultrasound lies above 20 kHz in the sound spectrum, is inaudible for humans utilized for diagnosis [23]. It plays an influential role in the medical domains such as Cardiology [24], Gynecology [25], Oncology [26], Obstetrics [27] etc. It does not involve any ionizing radiation and also a magnetic field for its operation which makes the ultrasound a non-destructive, affordable and also an efficient tool [28] [29] [30]. As illustrated in Figure 1, the structure of a conventional ultrasonic transducer is made up of an active material i.e. Piezo material, top and bottom electrodes to supply the AC voltage, a backing material, a matching layer for the acoustic impedance mismatch between two medium and acoustic lens in the front to focus the generated ultrasound beam [31]. The acoustic impedance is the measure of resistance experienced by the ultrasound. The larger the acoustic impedance, the better the reflection of the ultrasound. Therefore, a gel is used to match the impedance between the ultrasound and the respective test medium [30]. The ultrasonic transducer works under the principle of piezoelectricity which is discussed in Chapter 3. The piezoelectric element is the active part of the transducer. This element is



www.manaraa.com

sandwiched between the top and bottom electrodes. When the voltage is applied to the active element through the electrodes, stress is induced in the form of mechanical vibrations. This produces a pulse of ultrasound [32].

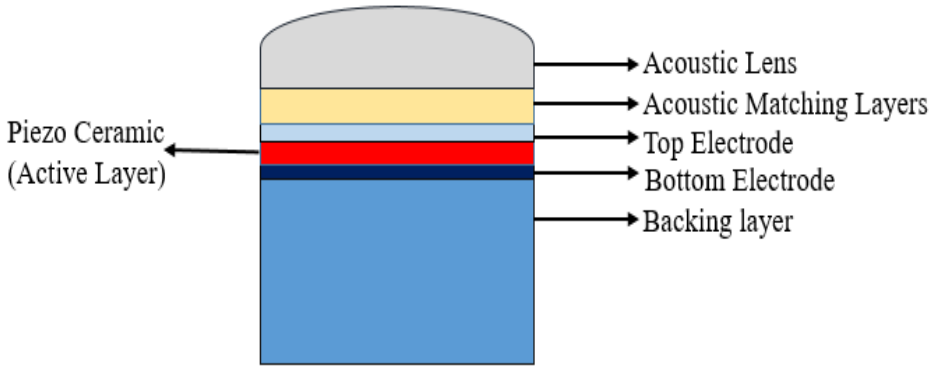


***Figure 1*** *Cross-sectional view of conventional ultrasound transducer. (Not to Scale).*

Based on the density of the tissue and the acoustic impedance of the medium, the speed of the transmission and the receiving of the ultrasound will alter. The transmitted ultrasound hits the targeted tissue and reflects back in the form of echoes. This principle is the pulse-echo method. The reflected ultrasound hits the transducer and produces voltages of small magnitude [30]. This excites the piezo material due to the piezoelectric effect. These echoes are fed into the electronic system such as band-pass filters, amplifiers and a data acquisition system such as microprocessor and Analog/Digital converter for signal processing. This signal is further converted to form an image for the patients. Different modes are used in the ultrasound for imaging. The 1D A-mode, and M-mode (M stands for motion) were the first used modes in the earliest transducers [33]. The resolution of the image is directly proportional to the number of transducer elements as this increases the output power of the ultrasound and determines the resultant image in real time as well [2]. Therefore, multiple elements are used to make 1D and 2D arrays. However, 2D imaging provides only flat images and does not give all the necessary information such as lateral and axial resolution



www.manaraa.com

of the target object and especially complex structures [34]. To overcome these limitations, 3D/4D imaging is developed. This method addresses the limitations of 2D imaging has served the medical field for more than three decades [35].

Despite developing advanced imaging, the fabrication limitations remain as a concerning issue because the conventional piezoelectric transducer fabrication process is based on the dice and fills approach. The process begins by dicing the piezo ceramic slab followed by sandwiching them between a top and a bottom electrode. Then the matching and backing layer is attached in the front and back respectively. A dicing saw is used to make a cut between the elements called kerf and those cells are put side by side to make arrays [36]. A lens is attached at the front as illustrated in Figure 1. The shape of the lens varies based on the requirements of the applications. The whole process is time-consuming and makes the structure bulkier for array configuration. This design is prone to electrical cross talk, high acoustic impedance and high noise level due to the high-frequency operations. This process of creating transducers challenges the batch fabrication and also other factors such as electromechanical coupling, quality factor, frequency bandwidth and design flexibility as well [37] [38] [39] . This can be overcome using the MEMS technology which is discussed in the next section.

## 2.7 Micromachined Ultrasound Transducer

As discussed in the previous section, conventional transducers are limited to fabrication, size, flexibility, acoustic impedance mismatches. These limitations can be overcome by employing Micromachined Ultrasound Transducers (MUT) which is a device made using MEMS technology. MUTs have membranes of micro or nano scale which is



www.manaraa.com

driven either piezoelectrically or capacitively. This high capability of miniaturization is offered by Micro-Electro Mechanical Systems (MEMS). MEMS is a technology which utilizes micro and nano fabrication techniques to develop and combine mechanical and electrical components in microscale [40] [41].

The fabrication process of the unconventional transducers makes it difficult to integrate different resonant frequencies and dimensions on a single chip. This is addressed by Micromachined Ultrasound Transducer (MUT) by offering design flexibility. It can be a promising alternative to the bulk transducers as the MUTs offer low power consumption, easy integration with electric circuits, mass production at low cost. Batch fabrication is possible because of MEMS due to the miniaturization capability [41] [42]. As mentioned before, based on the driving mechanism of the piezo material in the transducer, MUT is divided into Capacitive Micromachined Ultrasound Transducer (CMUT) and Piezoelectric Micromachined Ultrasound Transducer (PMUT) [43].

### 2.7.1 Capacitive Micromachined Ultrasound Transducer

Capacitive Micromachined Ultrasonic Transducer (CMUT) is considered as a viable alternative for the conventional piezoelectric transducers which offers wide bandwidth, large batch fabrication and higher frequency [44] [45]. As illustrated in Figure 2, The structure has two parallel plates separated by a vacuum cavity. A thin flexible conducting top plate which is the vibrating and moving membrane is separated from the fixed silicon substrate or bottom electrode by a vacuum cavity. On applying a DC bias voltage to the top and the bottom electrode, an electrostatic force is created between them. This force attracts the top electrode towards the bottom electrode which changes the



www.manaraa.com

capacitance of the CMUT. Due to the stiffness of the membrane, a mechanical restoring force is created against the downward motion. During a transmission mode, an alternating voltage is overlaid on the DC bias voltage, the top membrane starts to vibrate which results in the generation of the ultrasound. In receiver mode, the reflected ultrasound from the target tissue hits the top membrane. The membrane deflects which results in the change in capacitance and output. It can be converted to useful data for further processing [46].

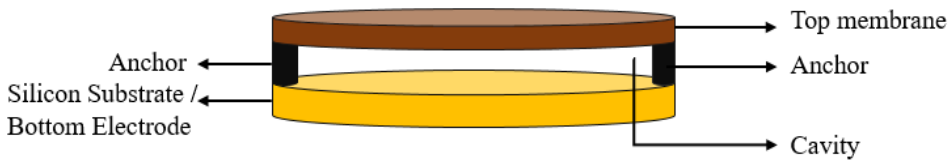


***Figure 2*** *A Schematic diagram of Capacitive Micromachined Ultrasound Transducer. (Not to Scale).*

The micromachining fabrication technique gives the flexibility to design the cavity in the range of sub microns giving CMUT the ability to offer wider bandwidth, low power consumption and cost [47]. The main disadvantage of the CMUT is the higher requirement of an input voltage. when the voltage is increased, the restoring force cannot balance the force further and collapses the entire structure. This voltage is known as the pull-in voltage The need for maintaining a small gap in CMUT limits the resonant frequency and the output pressure as the small gap height restricts the deflection of the top membrane [48]. Furthermore, the need for separate CMUT devices and external circuit for transmitting and receiving purposes increases the complexity of the structure [49] [50]. The disadvantages of the CMUT are overcome by another MUT which is discussed in the next section.



www.manaraa.com

## 2.7.2 Piezoelectric Micromachined Ultrasound Transducer

The limitations of conventional piezoelectric transducers in having a bulk structure are addressed by this promising development called Piezoelectric Micromachined Ultrasonic Transducer (PMUT) [51]. Unlike conventional transducers, PMUT is based on the flexural mode of operation which addresses and reduces the large acoustic impedance [52]. The structure of the PMUT consists of thin piezoelectric film ranging from 500nm to 1µm depending on the application requirements, sandwiched between the top and bottom electrodes. Both the piezoelectric film and the electrodes are mounted on a silicon substrate. When an AC signal is applied to the electrodes, the piezo material vibrates i.e. squeezes and expands. This phenomenon results in the generation of ultrasound [53]. Moreover, PMUT does not require gap or cavity for generating ultrasound which eliminates the limitations of the PMUT which is faced by and CMUT [54] [55] [56]. The following are the major differences between the conventional transducer and PMUT. First, the entire structure of PMUT is in the range of microns to a few millimeters which facilitate in achieving high frequency [57]. Second, the micromachining technique utilizes the physical and chemical properties of the silicon. This makes the PMUT structure flexible and enables batch fabrication. These facilitate the array structure in PMUT which in turn increases the overall acoustic power [52]. Finally, resonance is not influenced by the thickness of the layers as they are only a few hundred microns. This makes the PMUT independent of the thickness and makes PMUT a thin structure [58]. Despite facing low electromechanical coupling and narrow bandwidth, PMUT shows promising results in achieving affordable devices in batches [59]. The working mechanism, layer by layer



www.manaraa.com

analyses and the acoustic output pressure of the proposed PMUT is discussed in the upcoming chapters.

## 2.8 Conclusion

Worldwide, medical imaging plays a crucial role in the lives of humans. Therefore, the methodical approach and reliability are required in designing and developing imaging technologies. From the analyses of different imaging technologies, each technology has its pros and cons. Since this includes humans, a non-invasive and affordable imaging technique is required. Furthermore, PMUT is not only non-invasive but also addresses the major limitations of the conventional transducers. Though this is in the development phase, with proper optimization and modelling, it shows potential for further development.



www.manaraa.com

# Chapter 3

# Piezoelectric Micromachined Ultrasonic Transducer

*"Invention is the most important product of man's creative brain. The ultimate purpose is the complete mastery of mind over the material world, the harnessing of human nature to human needs."*

*-Nikola Tesla*

## 3.1 Introduction

The piezoelectric micromachined ultrasonic transducer is a propitious alternate to overcome the limitations of the conventional ultrasound transducer. The flexibility and simplicity offered by PMUT are one of the major reasons for this research focus. As discussed in the previous chapter, PMUT provides low acoustic impedance , low operating voltage, simple fabrication processes which makes it a potential candidate for medical imaging technology [58]. In this chapter, the working mechanism and the critical parameters are discussed in detail.

## 3.2 Operation Principle of PMUT

The operation of the PMUT obeys the piezoelectric effect [58]. The structure of the PMUT and the critical parameters are discussed in this section.

### 3.2.1 Fundamental Structure

In this thesis, the thin film Aluminum Nitride (AlN) based PMUT structure is designed and built based on fabrication process called PiezoMUMPs which is discussed in



www.manaraa.com

Chapter 6. The piezo material, AlN (500nm) is sandwiched between top electrode, Aluminum (1µm) and bottom electrode (1µm), Chrome (20nm). AlN is selected for its piezoelectric strain co-efficient, $d_{33}$, in the range of 3.9-5.5 (Pc/N) [60]. The entire structure is built on a silicon substrate as illustrated in Figure 3.

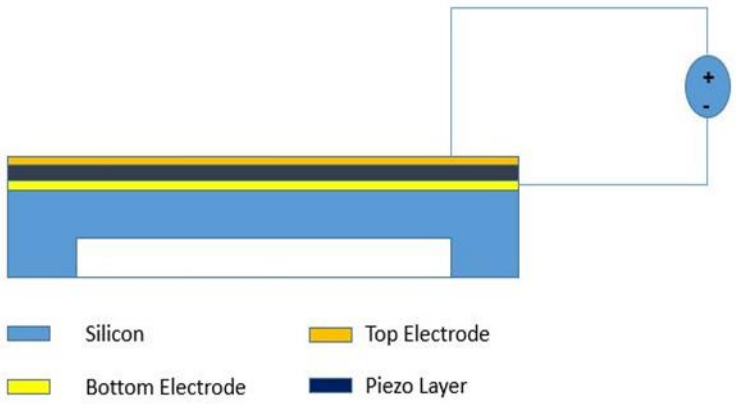


***Figure 3*** *Structure of Piezoelectric Micromachined Ultrasound Transducer (PMUT)*

The material properties of different layers are one of the factors which determine the resonant frequency of the structure. The most essential part in the structure of PMUT is the material properties, radius and thickness of the piezo layer. Firstly, the material properties such as piezoelectric, dielectric and elastic constants of the piezo layer as these determines the electromechanical coupling (k) of the PMUT and also the acoustic impedance. For instance, Lead Zirconate Titanium (PZT) has high k factor and is commonly reported material in PMUTs. The PZT is used in various sectors such as medicine, transportation, communications, etc. PZT is also available as ceramics and polycrystalline. The high thermodynamic variable in PZT makes it temperature independent. The other common materials are Polyvinylidene fluoride (PVDF) that is gradually replacing the PZT because it is light and highly flexible [61], AlN [62], and ZnO (Zinc Oxide) [63]. Secondly, the metals such as Chromium, Platinum, Aluminum are selected for electrodes as they have



www.manaraa.com

high conductivity. The preferred material to build the substrate is silicon as they are readily available, inexpensive. The high precision and reproducibility in fabricating the MEMS devices [60].

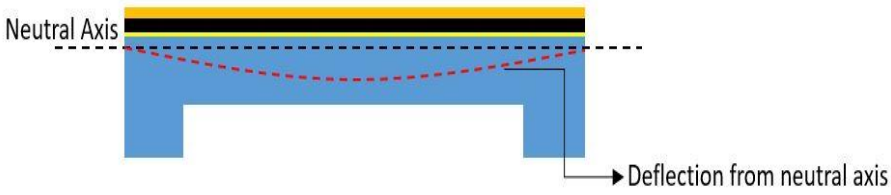


***Figure 4*** *PMUT with neutral axis and the deflection of the membrane from the neutral axis*

In this work, the unimorph PMUT is operated in $d_{33}$ mode. The electric field is applied to the top and bottom electrodes in z-direction which results in deflection from the neutral axis as illustrated in Figure 4. The plate vibration equation is given by Equation (1) [64],

$$D\nabla^2\nabla^2 w + I_0 \frac{\partial^2 w}{\partial t^2} = \nabla^2 M_p + P_{ext} \tag{1}$$

where D is the flexural rigidity of the plate given by Equation (2) [64],

$$D = \sum_{i=1}^{q} \frac{Y_i}{3(1-v_i^2)} [(z_i - z_N)^3 - (z_{i-1} - z_N)^3] \tag{2}$$

with surface density $I_0$ by Equation (3),

$$I_0 = \sum_{i=1}^{q} \rho_{ih_i} \tag{3}$$



www.manaraa.com

This PMUT design is a clamped plate structure which is optimized and analyzed for higher acoustic output and desired resonant frequency. Three different structures of circular, square and rectangular PMUT have been designed and analyzed which is discussed in Chapter 4.

## 3.2.2 Piezoelectric Effect

Each molecule in an object has its own gravity centers for positive and negative charges. Under the absence of pressure/force, these gravity centers of both the charges coincide as shown in Figure 5(a). But when a force/pressure is exerted on the molecule, the gravity centers of the charges separate and forms a dipole. This process is called polarization as shown in Figure 5(b) and 5(c).

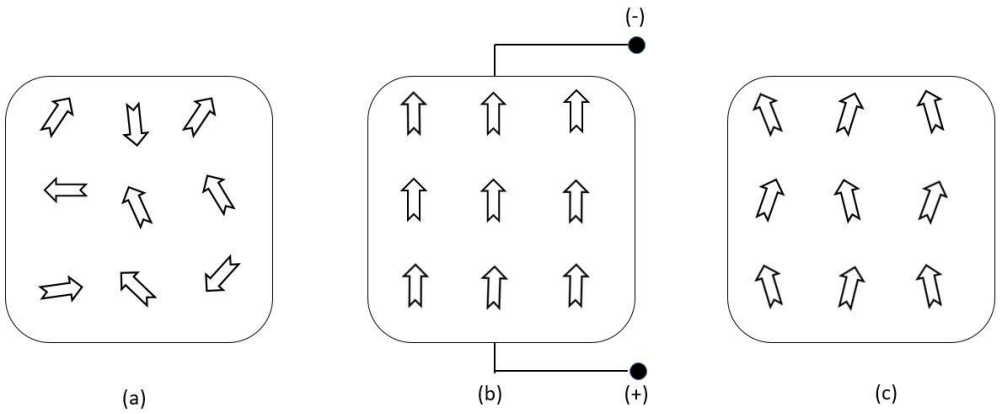


***Figure 5*** *The polarization process of a piezoelectric material. (a) The orientation of the positive and negative charges in the absence of an external electric field. (b) The alignment of the charges when an electric field is applied. (c) The net polarization after the removal of the electric field.*

The electrodes are attached on top and bottom surface of the piezo layer. On the application of force/pressure, polarization makes the charges to touch the electrodes. The negative charges are attracted to the positive terminal and vice versa. On removal of the external pressure, the charges go into their equilibrium state. The entire process is repeated which converts the mechanical energy into electrical energy. This is called as direct piezoelectric



www.manaraa.com

effect. The reverse mechanism of the same process is called the inverse piezoelectric effect and this effect is responsible for the generation of ultrasound in PMUT when an AC signal is applied [65].

### 3.2.3 Equivalent Circuit Model

Designing an appropriate equivalent circuit model is an essential process which has to be done to attain the compete transducer system representation. With a proper equivalent circuit model, the circuit designer can optimize the front and back end processing and design. This influences the overall efficiency of the transducer system. In this section, a mechanical and an electrical equivalent circuit model is developed for a single cell [64].

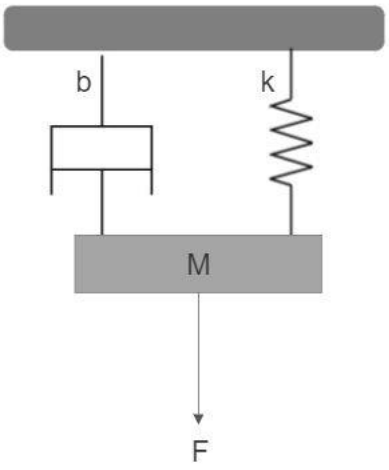


***Figure 6*** *Mechanical equivalent model of PMUT using Mass-Spring-Damper Model*

The mechanical equivalent model of the PMUT can be modelled using the mass-spring-damper model as shown in Figure 6. The external force, F oscillates the mass, M which is attached to the spring k and a damper b. When an alternating voltage is applied to the electrodes, a mechanical force is generated by the piezo layer due to the piezoelectric effect.



www.manaraa.com

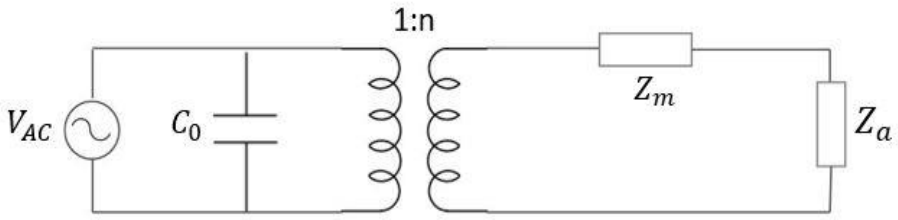


***Figure 7*** *Electrical equivalent circuit of PMUT*

The stiffness of the membrane counteracts the mechanical force which results in the deflection of the membrane. As illustrated in Figure 7, the impedance of the capacitor ($C_0$) defines the electrical impedance i.e. the impedance formed the piezo layer of the PMUT. The structure of the vibrating plate defines the mechanical impedance ($Z_m$) of the PMUT. The $Z_a$ defines the acoustic domain and can be written as shown in Equation (4),

$$Z_a = R_a + j\omega L_a \tag{4}$$

where $R_a$ is the damping of the medium and $L_a$ is the acoustic mass. The electromechanical coupling i.e. coupling of the electrical and mechanical domains is represented, n, which determines the symmetrical working operation at both the transmitting and receiving part of the transducer. It the direct measure of efficiency of the PMUT. The K factor can be written as shown in Equation (5),

$$k^2 = \frac{f_a^2 - f_r^2}{f_a^2} \tag{5}$$

where the $f_r$ *and* $f_a$ is the resonant and anti-resonant frequencies respectively [66] [67].



www.manaraa.com

## 3.3 Resonant Frequency

The applied AC signal excites the structure to vibrate at multiple frequencies. The amplitude of the vibration attains the maximum at a specified frequency of operation. That frequency gives the maximum vibration, known as the resonant frequency. The working operation of the PMUT relies on this resonant frequency. The critical parameters such as radius and thickness of the layer, material properties and the applied voltage determines the resonant frequency of the respective structure. As the resonant frequency lies close to the natural frequency of the structure, the above said parameters are optimized to attain the maximum efficiency of the PMUT [58] [68]. In this work, layer by layer analyses has been done to analyze the effects of parameters on the resonant frequency. The resonant frequency of a multi-layer structure which is clamped on all edges is given by Equation (6) [64],

$$f_r = \frac{\gamma_1^2}{2\pi R^3}\sqrt{\frac{D}{\mu}} \tag{6}$$

where $\gamma = 3.19$ for fundamental resonance mode, D is the flexural rigidity and $\mu$ is the mass per given area as shown in Equations (7) and (8) [64],

$$D = \frac{1}{3}\sum_{i=e}^{top} E_i \frac{(t_i - z_n)^3 - (t_{i-1} - z_n)^3]}{(1 - v_i^2)}. \tag{7}$$

and

$$\mu = \sum_{i=e}^{top} \rho_i t_i \tag{8}$$



www.manaraa.com

where the $\rho_i$, the density of the layer, $t_i$, thickness, $E_i$, Young's modulus and $v_i$, the Poisson ration of the layer.

## 3.4 Acoustic Power

The resonant frequency is one of the critical parameters which determines the acoustic performance of the PMUT. Since PMUT is relatively a narrow bandwidth [59], it should be operated at the respective resonant frequency to deliver a maximum output pressure and to achieve large penetration depths. Moreover, the resultant output pressure is directly proportional to the applied voltage. The PMUT operates at lower voltages which provides low power consumption and also prevents the repolarization of the charges in the piezo layer. In conventional transducers, the acoustic impedance between the structure and the testing domain such as air, water, skin, metal etc., downturn the acoustic output performance of the system. The acoustic impedance between the ceramic and the test domain should match as it increases the efficiency of the PMUT. Even though the implementation of the matching layers with quarter wavelength solves the limitation, the complexity of the fabrication process increases and also alters the resonant frequency of the structure. However, in PMUT, low acoustic impedance can be achieved by optimizing the critical parameters and the micromachining techniques that allows the fabrication of thin films [58]. The radiation boundary conditions, sound pressure level and acoustic output pressure are investigated in Chapter 5 using FEA simulations.

## 3.5 Conclusion

In this chapter, the physics involved in the working operation of the PMUT such as fundamental structure, effect of piezoelectricity in transmitting and receiving the signal,



www.manaraa.com

electromechanical coupling function using equivalent circuits are studied. Furthermore, the governing equations and critical parameters of the fundamental structure and resonant frequency of the PMUT are also studied. However, the complexity of analytical modelling increases with added layers with different thicknesses in the structure. The fundamental equation for the resonant frequency is prone to error when more than one material or layer is added in the structure of PMUT. Moreover, the complications in calculating in real-time values for an array configuration of PMUT is liable to err. The above-mentioned limitations and the critical parameters of PMUT are further extensively investigated in the next chapter by conducting FEA simulations.



www.manaraa.com

# Chapter 4

# Critical Design Parameters and Electrical Analyses of PMUT

*"Everything that informs us of something useful that we didn't already know is a potential signal. If it matters and deserves a response, its potential is actualized."*

*- Stephen Few*

## 4.1 Introduction

An alternating voltage is applied between the top and bottom electrodes of the PMUT which facilitates excitation of the piezo layer. As discussed in section 3.3, the maximum excitation of the piezo layer can be observed at its natural vibration frequency called the resonant frequency. Moreover, to attain the maximum efficiency of the PMUT, the device must be operated in its respective resonant frequency. As shown in Equation (9), the critical parameters such as flexural rigidity, density, thickness and radius of each layer can be analyzed and optimized to get the resonant frequency of the PMUT. A resonant frequency analyses for the proposed PMUT, the critical design parameters and electrical analyses are presented, studied and evaluated in this chapter. As discussed in section 3.5, analytical modelling becomes complex for structures with different thicknesses. The deviation of the simulated values from the calculated values of simple and complex structures is discussed in section 4.2.1. The electrical analyses for different radii, thickness and shape are studied and investigated in this chapter.



www.manaraa.com

## 4.2 Finite Element Analyses

A numerical technique is employed to evaluate the physical entities and phenomenon. This process is called Finite Element Analyses (FEA). In FEA, the mathematical model is described using Partial Differential Equations (PDEs) and these equations are solved using FEM and that provides engineers and researchers with the information such as resonant frequency, pressure distribution and sensitivity analyses about the respective simulated model.

### 4.2.1 COMSOL Multiphysics – Electrical Simulations

In this thesis, COMSOL Multiphysics Version 5.5 software is utilized to perform FEA simulations and analyses of PMUT. Critical parameters of the PMUT are investigated thoroughly in this chapter. COMSOL offers numerous physical solvers and the option to couple multiple physics interface modules such as acoustics, electromechanics, fluid flow and heat transfer. In this chapter, the "Eigen frequency, Prestressed" and "Frequency domain" studies are performed using the MEMS module consisting of solid mechanics and electrostatics. The electrical boundary conditions and the determination of resonant frequency for proposed geometries of the PMUT are discussed under their respective geometries. The software is operated on a Windows machine consisting of 2 GHz, 16 cores Intel Xenon with a RAM speed of 384 GB.

### 4.2.2 Domain Meshing

Identifying the mesh type plays an integral part in modelling the PMUT. The meshing is essential when the structure has layers with thicknesses of different orders. The simulated devices in this thesis range from 500nm to 10µm. Therefore, an appropriate mesh



www.manaraa.com

setting must be done by considering all range of thicknesses in the structure. COMSOL offers customizable meshing which is used to divide the entire structure into smaller domains, called solved data points. These smaller domains are further divided into elements.

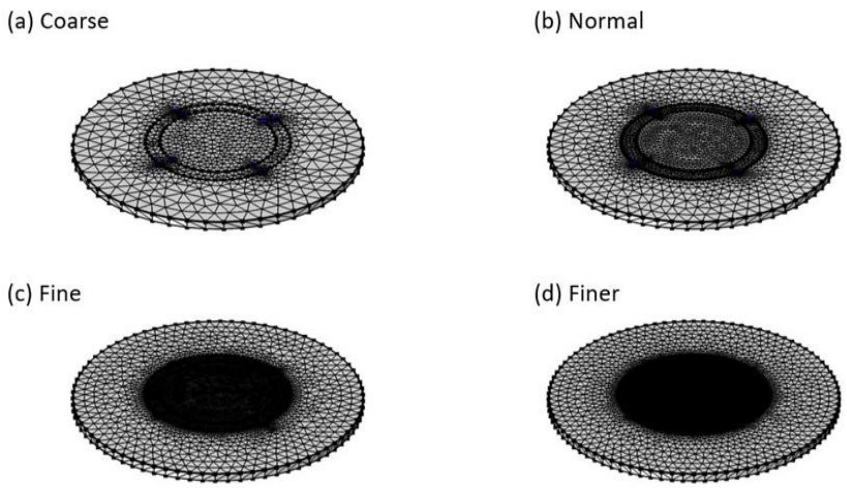


***Figure 8*** *Different types of Meshing in COMSOL.*

Based on the size of the element, the mesh is classified as coarse, coarser, extra and extremely coarse, normal, fine, finer, extra and extremely fine. The coarse meshing has a lower density whereas the extremely fine meshing has the higher density. Here the density denotes the number of elements in a domain. Figure 8 shows an increase in the number of elements for each mesh type. However, the denser mesh tends to increase the computational time and memory size. Therefore, suitable mesh type is required for efficient simulation. The simulated PMUT presented in Figure 8 has a top electrode (Al) of 95µm radius, a piezo layer of 115µm radius and silicon substrate of 165µm radius. As discussed in section 3.3, the PMUT must be operated at its resonant frequency to attain the maximum



www.manaraa.com

transduction. Therefore, eigen frequency study is conducted to evaluate to determine the respective resonant frequency of the structure.

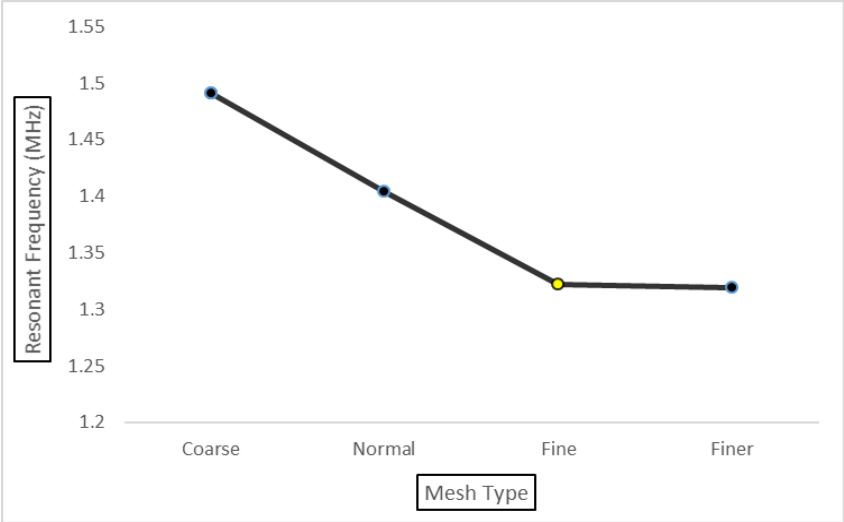


***Figure 9*** *COMSOL simulation results showing the trend of the resonant frequency with the respective mesh type.*

To select the suitable mesh, the resonant frequency must be independent of the change in mesh setting. Figure 9 illustrates the relationship between the resonant frequency of the PMUT and mesh type. The graph depicts that the resonant frequency becomes independent of the meshing at the "Fine" mesh. Therefore, fine mesh is chosen to simulate the PMUT devices in this chapter. In this thesis, layer by layer analyses has been done to determine the resonant frequency of the designed PMUT. Boundary conditions define the functionality to be applied to that selected domain and discussed under their respective sections.

## 4.3 Parametric analyses of Piezo layer

The piezo layer as shown in Figure 10 is analyzed by changing the radius, thickness and applied voltage and examining the effect on resonant frequency. The FEA simulation



www.manaraa.com

results are compared with the analytical model results to validate the accuracy of the simulation modelling.

### 4.3.1 Boundary Conditions

This is called the Step-I analyses where only the piezo layer is investigated. As illustrated in Figure 10, the top surface of the piezo layer is selected as the terminal where the AC voltage is applied to activate the device. The bottom surface of the piezo layer is selected as ground.

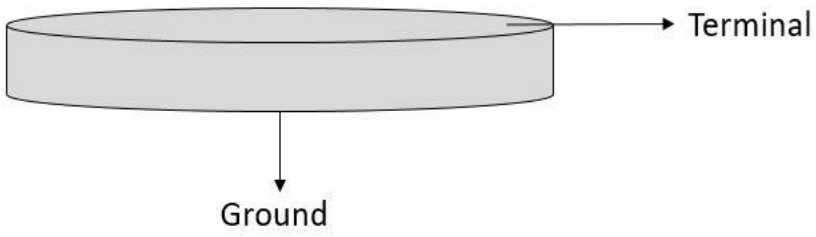


***Figure 10*** *The boundary conditions of Step I – Piezo layer analyses. The top surface is selected as terminal and the bottom surface is selected as ground.*

The edges are fixed to create a clamped structure. Both the top and bottom surface of the piezo layer is selected as a free domain for the structure to vibrate in the longitudinal direction.

### 4.3.2 Effect of the Radius

The radius is one of the critical parameters which has a substantial effect in determining the resonant frequency of the PMUT. As shown in Figure 10, only the piezo layer is designed and simulated for analyses. Equation (9) is used to calculate the resonant frequency for simpler structures.



www.manaraa.com

$$f_r = 0.5\,\frac{t}{a^2}\sqrt{\frac{E}{\rho}} \tag{9}$$

The material Aluminum Nitride with Young's modulus (E) of 348 GPa and density ($\rho$) of 3300 kg/$m^3$ are selected for analyses purposes. The radius of the piezo layer is investigated from 10µm to 200µm in incremental value of 50µm. The thickness of the piezo layer is 2µm and the applied AC voltage 50V is selected for analyses as given in Table II.

***Table II*** *Parameters used in investigating the effect of radius on piezo layer*

| | Piezo layer radius (µm) |
|---|---|
| Applied AC voltage – 50V<br>Piezo layer thickness - 2µm | 50 |
| | 100 |
| | 150 |
| | 200 |
| | 250 |

As per the equation (9), the area of the layer is inversely proportional to the resonant frequency. From Figure 11, it is clear that the resonant frequency decreases with the increase in the radius of the piezo layer. In order to corroborate the simulation results, the resonant frequency is calculated with the aforementioned material properties and radii.

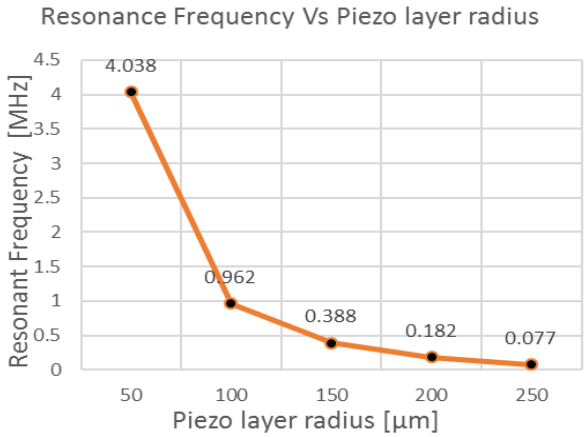


***Figure 11*** *This graph is plotted between simulated resonant frequency values and radius of the piezo layer. An alternating voltage of 50V is applied to the layer of a thickness 2µm.*



www.manaraa.com

The simulation and calculated results are compared using the MATLAB. As shown in Figure 12 the trend of the calculated and simulated results makes a similar curve. This substantiates that the radius of the layer is inversely proportional to the resonant frequency and also the accuracy of the simulation results.

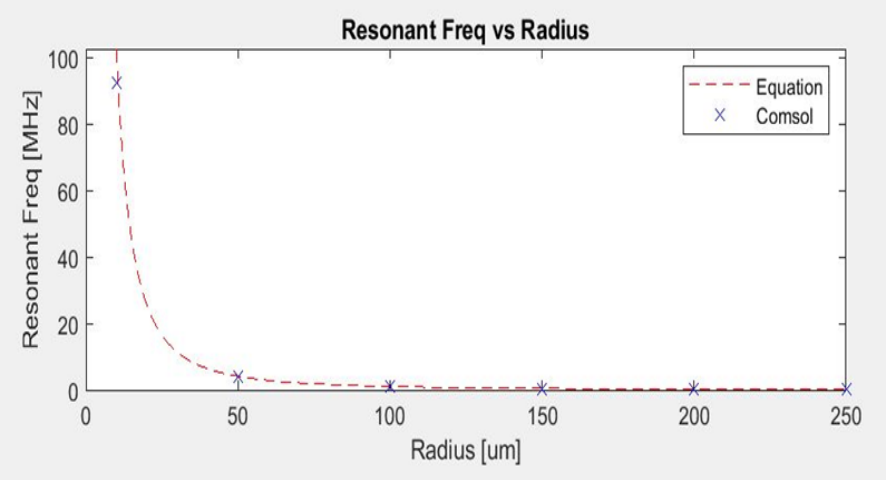


***Figure 12*** *The graph showing a similar curve for calculated and simulated resonant frequency plotted for a piezo layer of thickness 2µm for an alternating voltage of 50V.*

## 4.3.3 Effect of the Thickness

One of the factors that influence the resonant frequency of the PMUT is thickness. In order to investigate the effect of the thickness on the performance of the proposed PMUT, the structure is modelled and simulated as shown in Figure 13. The resonant frequency is calculated based on Equation (9) to investigate the values of the thicknesses. The material Aluminum Nitride (AlN) with Young's modulus of 348 GPa and density of 3300 kg/$m^3$ is selected for a fair comparison with the developed device. The thickness of the piezo layer is analyzed from 1µm to 6µm in incremental value of 1µm. A wide range of thickness values is picked to analyze and understand the effect on the resonant frequency. The radius of the piezo layer is 50µm and the applied AC voltage is 50V selected and fixed for analyses as given in Table III. As per the equation (9), it can be seen



www.manaraa.com

that the thickness of the piezo layer is directly proportional to the resonant frequency. From Figure 13, it is observed that the resonant frequency increases with the increase in the thickness of the structure. Moreover, this increases the flexural rigidity of the structure. Because the thicker structure restricts the bending moment which in turn affects the resonant frequency.

***Table III*** *Parameters used in investigating the effect of thickness on piezo layer*

| | Piezo layer thickness (µm) |
|---|---|
| Applied AC voltage – 50V<br>Piezo layer radius - 50µm | 1 |
| | 2 |
| | 3 |
| | 4 |
| | 5 |
| | 6 |

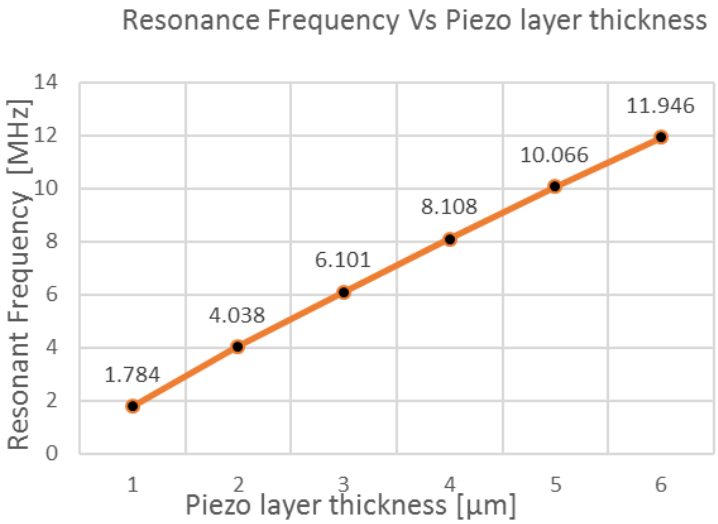


***Figure 13*** *This graph is plotted between simulated resonant frequency values and piezo layer thicknesses. An alternating voltage of 50V is applied to the layer of a radius 50µm.*

The simulation results are compared with the calculated resonant frequency and the graph is plotted using the MATLAB as shown in Figure 14. The values of the calculated and simulated results agree with each other, validating the proposed and simulated Multiphysics model that can be further developed into the PMUT complex geometry. This



www.manaraa.com

study indicated that the thickness is directly proportional to the resonant frequency and needs to be considered in the PMUT design for the target frequency range.

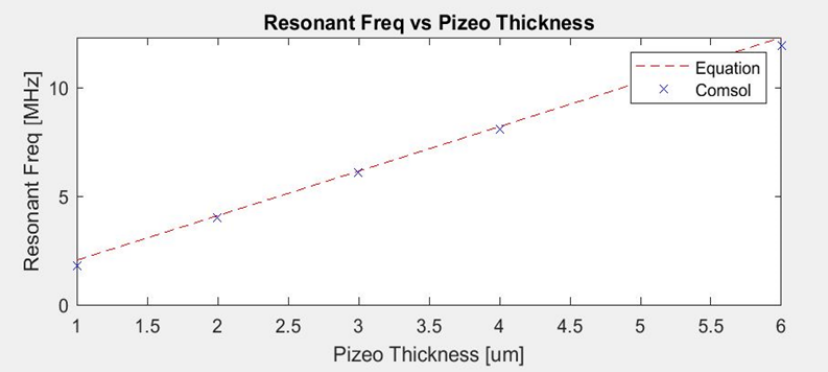


***Figure 14*** *The graph showing a similar curve for calculated and simulated resonant frequency plotted for a piezo layer of radius 50µm for an alternating voltage of 50V.*

## 4.4 Parametric analyses of Piezo layer and Silicon substrate

For the more complex structure of PMUT, the piezo layer with silicon substrate as shown in Figure 15 is analyzed by investigating the critical parameters. The effect of the addition of a layer on resonant frequency is investigated by comparing the simulated and calculated resonant frequencies from the general piezoelectric equations that hold for one-layer structure.

### 4.4.1 Boundary Conditions

This is called the Step-II analyses where a silicon substrate is added below the piezo layer. As shown in Figure 15, the AC voltage is given to the top and bottom surface of the piezo layer. The edges of both the piezo layer and silicon substrate are fixed and the top and bottom surfaces of both the layers are selected as a free domain to resample the MEMS



www.manaraa.com

movement. In order to evaluate the effect of adding a layer to the piezo layer is investigated and analyzed in this section.

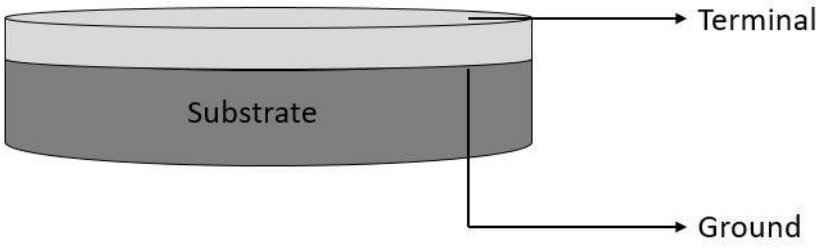


***Figure 15*** *The boundary conditions of Step II – Piezo layer and Silicon substrate analyses. The top and bottom surface of the piezo layer is selected as terminal and ground respectively.*

## 4.4.2 Effect of the Radius

In Step-II analyses, the material Aluminum Nitride with Young's modulus of 348 GPa and density of 3300 kg/$m^3$ along with Silicon with Young's modulus of 180 GPa and density of 2329 kg/$m^3$ is selected that resemble the more complex structure of PMUT. The radius of both the piezo layer and silicon substrate is the same as this is the case in the developed PMUT. As given in Table IV, the radius is investigated from 10µm to 250µm in incremental value of 50µm. The applied voltage is 50V and the thickness of the piezo layer and silicon substrate is fixed in 1:2 ratios. i.e. the piezo layer is 1µm and the silicon substrate is 2µm thick.

***Table IV*** *Parameters in investigating the effect of radius on the piezo layer and silicon*

| | Piezo and silicon layer radius (µm) |
|---|---|
| Applied AC voltage – 50V<br>Piezo and silicon layer thickness - 3µm | 50 |
| | 100 |
| | 150 |
| | 200 |
| | 250 |



www.manaraa.com

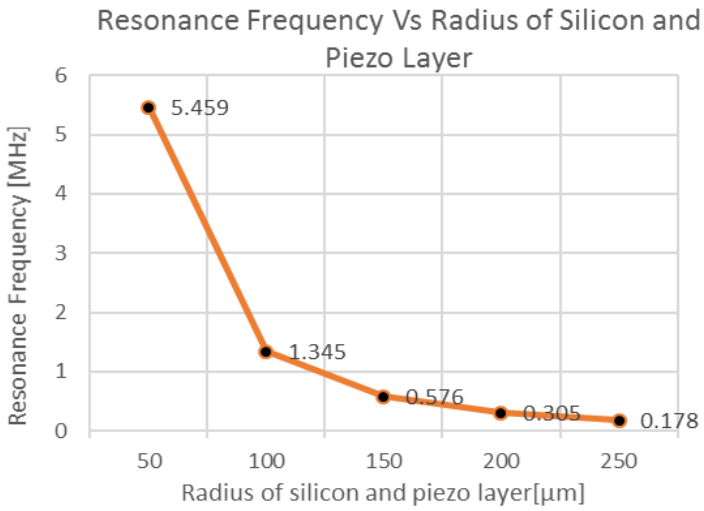


***Figure 16*** *This graph is plotted between simulated resonant frequency values and radii of the piezo layer and silicon substrate. An alternating voltage of 50V is applied to the structure of thickness of 3µm.*

The lowest radius of 50µm and highest of 250µm is selected to investigate the effect of the radius at the extreme values feasible for PMUT fabrication process proposed in this thesis. From Figure 16, the graph shows a significant drop in the resonant frequency with the increase in the radius of both layers. Considering this, 100µm is selected as the initial radius to design a low-frequency PMUT. Figure 17 illustrates that there is an inappreciable deviation of the calculated values from the simulated values. This negligible difference is due to the material properties of Aluminum Nitride and Silicon.

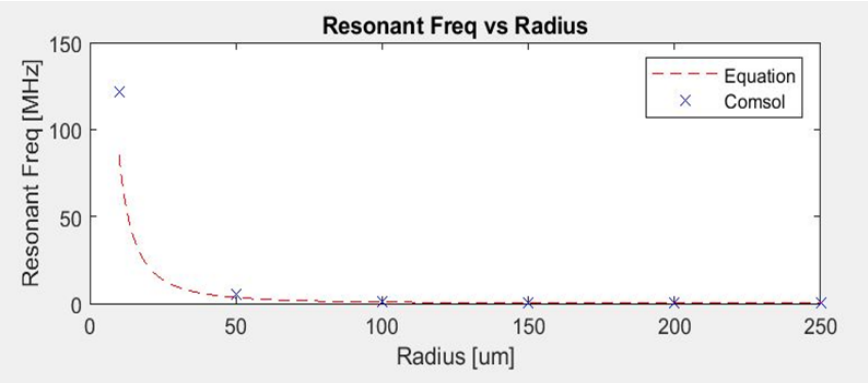


***Figure 17*** *The graph showing a slight deviation in the curve of calculated and simulated resonant frequency plotted for structure with thickness 3µm for an alternating voltage of 50V.*



www.manaraa.com

## 4.4.3 Effect of the Thickness

As discussed in section 4.3.2, Equation (9), is used to calculate the resonant frequency of a one-layer piezo structure. However, the complex structure of PMUT includes several layers and the material properties of both the Aluminum Nitride and Silicon are included in the calculation of Young's Modulus and Density. The thickness analyses have been done in two approaches. The first is to analyze the effect of thickness by investigating the thickness of the piezo layer and the latter is by studying the thickness of the silicon substrate as given in Table V.

***Table V*** *Parameters used in investigating the effect of thickness on the piezo layer in piezo/silicon structure*

| | Piezo layer thickness (µm) |
|---|---|
| Applied AC voltage – 50V<br>Piezo and silicon layer radius - 50µm<br>Silicon layer thickness - 2µm | 1 |
| | 2 |
| | 3 |
| | 4 |
| | 5 |

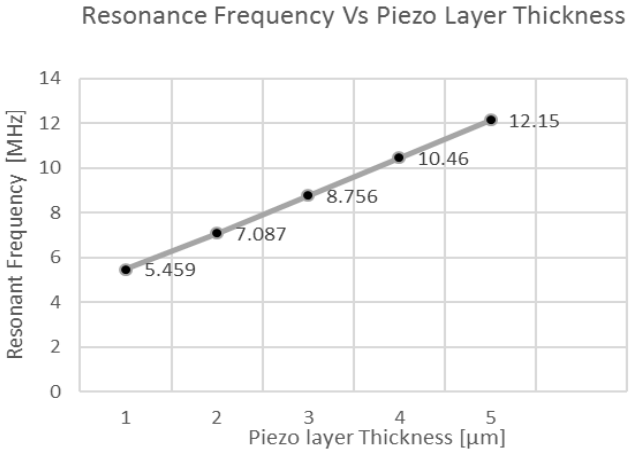


***Figure 18*** *This graph is plotted between simulated resonant frequency values and piezo layer thicknesses. An alternating voltage of 50V is applied to the layer of a radius 50µm.*

The first approach involves the variation of the thickness of the piezo layer from 1µm to 5µm and by fixing the applied voltage to 50V and silicon layer thickness as 2µm. As Figure



www.manaraa.com

18 depicts, the resonant frequency increases with the increase in the thickness by obeying Equation (9). As given in Table VI, the second approach involves the variation of the thickness of the silicon substrate by the values 1µm, 2µm, 10µm, 20µm and 30µm. The first two values are picked to analyze the 1:2 ratios as discussed in section 4.4.2. The 10µm is selected to evaluate the thickness effect based on the PiezoMUMPs design which is discussed in Chapter 6. The 20µm and 30µm are selected to observe the outcome of the resultant resonant frequency for thick PMUTs.

***Table VI*** *Parameters used in investigating the effect of thickness on the silicon layer in piezo/silicon structure*

| | Piezo layer thickness (µm) |
|---|---|
| Applied AC voltage – 50V<br>Piezo and silicon layer radius - 50µm<br>Silicon layer thickness - 1µm | 1 |
| | 2 |
| | 10 |
| | 20 |
| | 30 |

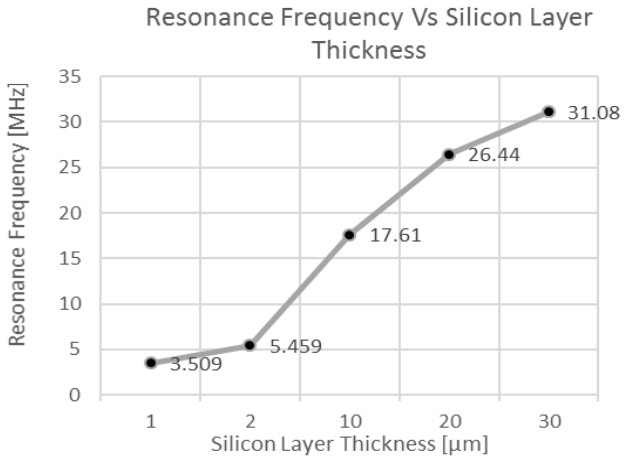


***Figure 19*** *This graph is plotted between simulated resonant frequency values and silicon layer thicknesses. An alternating voltage of 50V is applied to the layer of a radius 50µm.*

As Figure 19 depicts, the unvarying results have been observed. Furthermore, the simulated values are compared with the calculated values of the resonant frequency. From Figure 20, it is clear that there is a significant deviation of the calculated values from the simulated



www.manaraa.com

values. There are multifarious factors that contribute to this deviation. For instance, Equation (9) considers only Young's modulus and density of one material in a simple one-layer structure. The equation does not hold anymore for complex structures with added layers. Therefore, the response deviates from the existing simple formula.

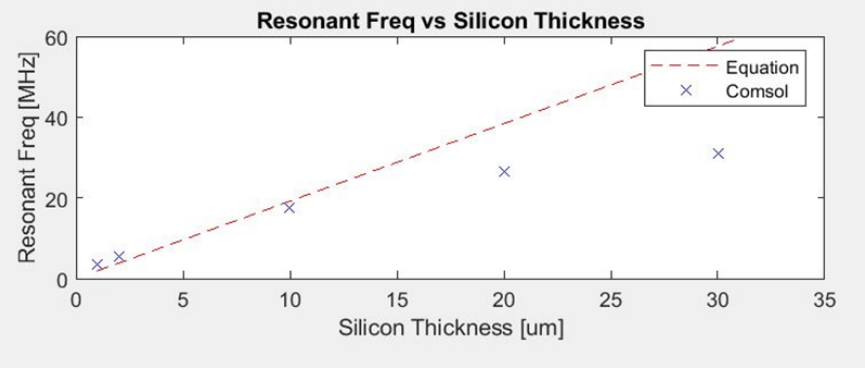


*Figure 20 A graph showing a significant deviation in the curve f calculated and simulated resonant frequency plotted for structure with thickness 3μm for an AC voltage of 50V.*

However, the proposed PMUT is a more complex structure that employs several layers of different geometries. COMSOL is a powerful tool which involves multifarious factors, for instance, residual stress, Electrical conductivity, Coefficient of thermal expansion by default. This authenticates the exactness of the results which is further investigated in the next section.

## 4.5 Parametric analyses of proposed Circular PMUT

A comprehensive analysis has been done to evaluate the effect of critical design parameters. However, the structure discussed in section 4.3 and 4.4 is not the complete PMUT. Therefore, the proposed design of PMUT is investigated in this section and it is based on a fabrication process, PiezoMUMPs. There are few design constraints such as fixed values for thicknesses. One of the critical design parameters, radius, is selected and analyzed based on the aforementioned step by step analyses to design the target low-



www.manaraa.com

frequency PMUT for better efficiency. The designs discussed in this section and 4.6 are fabricated and packaged which is discussed in Chapter 6.

### 4.5.1 Boundary Conditions

This is one of the designs of PMUT geometries. This is called the Design-I, modelled based on the design rules of a fabrication process called PiezoMUMPs. The thickness of the entire structure is fixed by the design rules which are discussed in Chapter 6. Moreover, the active areas in the structure of PMUT i.e. vibrating areas are only considered for simulation purposes. Therefore, the modelled PMUT is not an exact depiction of the fabricated PMUT. However, the passive areas are also simulated and compared to substantiate the point that there are insignificant changes in the results with or without the incorporation of passive layers in the simulations.

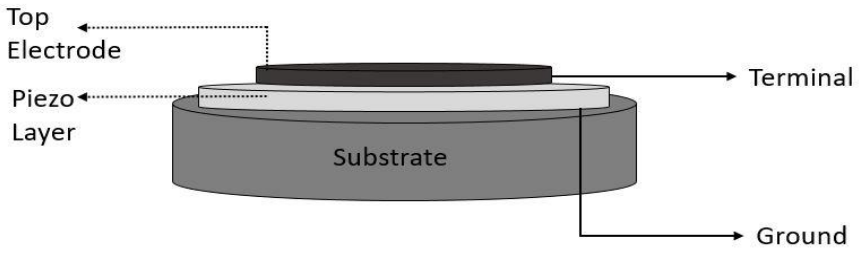


***Figure 21*** *The boundary conditions of the proposed design, circular PMUT. The top electrode is selected as terminal and the bottom surface of the piezo layer is selected as ground. The structure is built on a silicon substrate. The simulated design has a top electrode and bottom surface of the piezo layer to apply terminal and ground.*

As shown in Figure 21, the AC voltage is applied to the top electrode whereas the ground is applied at the bottom surface of the piezo layer. The entire structure is clamped at the edges. The top surface of the top electrode and the bottom surface of the silicon substrate is selected as free domains to facilitate the vibrations in the longitudinal directions. The



www.manaraa.com

parameters of the proposed circular PMUT are listed in Table VII. These are the parameters defined to design the circular PMUT whereas the thickness of each layer is fixed by the PiezoMUMPs. However, the radius is selected based on the step by step analyses to attain a lower resonant frequency range.

***Table VII*** *The parameters list such as radius, thickness and applied voltage for the proposed design, circular PMUT. The same parameters can be used for rectangular and square PMUT by changing the radius.*

| Name of the parameter | Value[unit] | Description |
|---|---|---|
| Vac | 1[V] | Applied AC voltage |
| r | 115,170,205,250 [µm] | Range of varied radii of the piezo layer(AlN) |
| r_Al | r-20[µm] | Radius of the top electrode (Al) |
| r_Si | r+50[µm] | Radius of the Silicon substrate |
| r_SiO2 | r_Si-10[µm] | Radius of Silicon dioxide |
| t_Al | 1.02[µm] | Thickness of the top electrode (Al) [Fixed] |
| t_AlN | 500[nm] | Thickness of the Aluminum Nitride [Fixed] |
| t_Si | 10[µm] | Thickness of the silicon substrate [Fixed] |
| t_SiO2 | 1[µm] | Thickness of the silicon substrate [Fixed] |

### 4.5.2 Effect of the Radius

The objective of this thesis is to design a low-frequency PMUT for higher penetration of the signal to reach the deeper tissues of the targeted area in the human body. The outcome is measure using a pulse-echo method where noise is unwanted. Due to low-frequency PMUTs, lesser noise is observed at the outcome.



www.manaraa.com

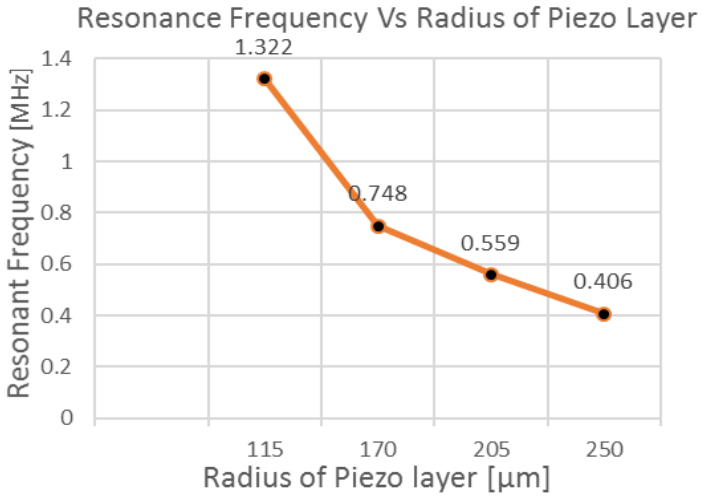


***Figure 22*** *This graph is plotted between simulated resonant frequency values and radii of the piezo layer for the circular PMUT for an alternating voltage of 1V.*

From section 4.3 and 4.4, it is clear that the radius must be higher than 50µm. Therefore, the proposed circular PMUT can be designed to operate at less than or equal to 1.5 MHz. The critical parameters mentioned in Table VII, have been optimized accordingly for the aforementioned resonant frequency. As Figure 22 illustrates, the resonant frequency decreases with an increase in the radius of the piezo layer.

## 4.6 Parametric Analyses of Square and Rectangular PMUT

The square and rectangular PMUT are also investigated as a Figure of merit and to investigate the effect of the geometry of the resonant frequency as well as power generation ability. Both shapes are designed and simulated based on PiezoMUMPs design rules. The effect of radius on the resonant frequency is investigated for both the shapes.

### 4.6.1 Boundary Conditions

As discussed in section 4.5, the same structure is designed but in a different shape. From Figure 23(a) and 24 (a), a similar structure, i.e. the entire structure is built on a silicon



www.manaraa.com

substrate. The simulated design has a top electrode and bottom surface of the piezo layer to apply terminal and ground. The top electrode is selected as terminal and the bottom surface of the piezo layer is selected as ground. The active areas are identified from section 4.3 and 4.4. Therefore, only the top electrode is built on the surface of the piezo layer. As illustrated in Figure 23 (b) and 24 (b), the AC voltage is applied to the top electrode whereas the ground is applied at the bottom surface of the piezo layer.

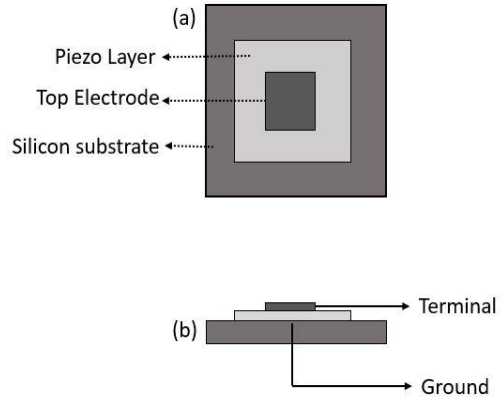


***Figure 23*** *The boundary conditions of the proposed design, square PMUT.*

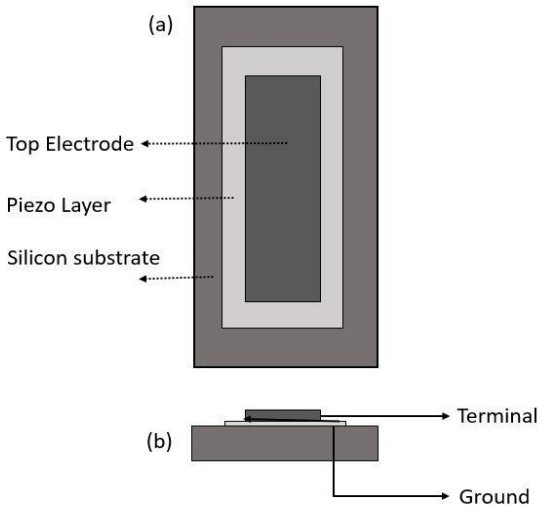


***Figure 24*** *The boundary conditions of the proposed design, rectangular PMUT.*



www.manaraa.com

As illustrated in Figure 24 (a) and (b), the simulated design has a top electrode and bottom surface of the piezo layer to apply terminal and ground. The top electrode is selected as terminal and the bottom surface of the piezo layer is selected as ground.

## 4.6.2 Effect of the Radius

The width and length of the rectangle are converted to areas and plotted as X-axis.

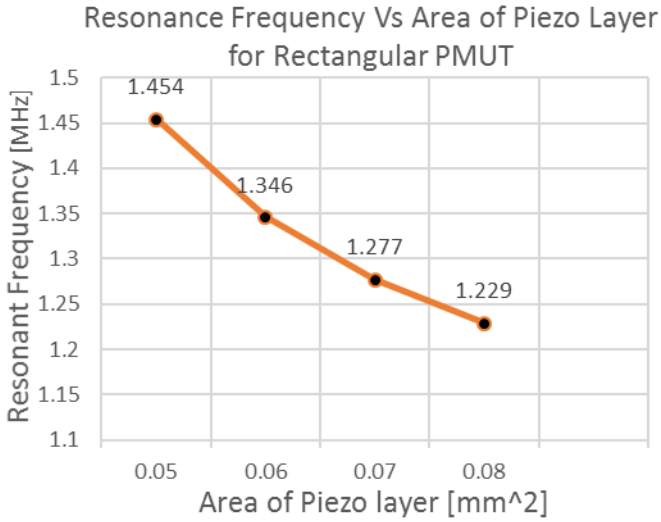


***Figure 25*** *This graph is plotted between simulated resonant frequency values and radii of the piezo layer for the rectangular PMUT for an alternating voltage of 1V.*

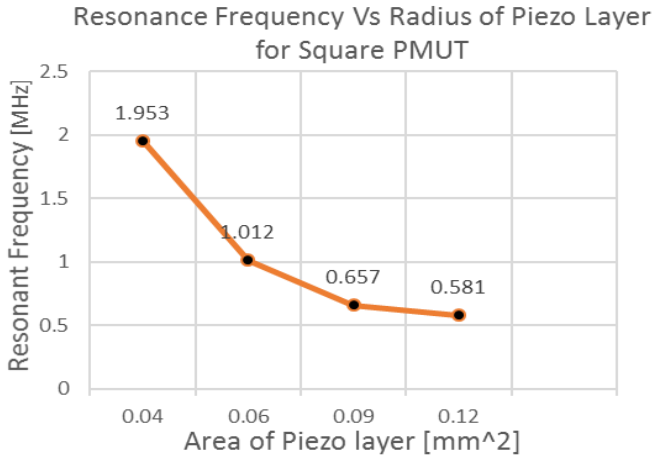


***Figure 26*** *This graph is plotted between simulated resonant frequency values and radii of the piezo layer for the square PMUT for an alternating voltage of 1V.*



www.manaraa.com

As mentioned in Table VII, the area is investigated, and the resonant frequency is simulated and plotted as Y-axis. As Figure 25 depicts, the highest resonant frequency is 1.45 MHz for an area of 0.05 $mm^2$. The third shape, Square, is selected for fabrication. From Figure 26, it is clear that the resonant frequency is 1.95MHz for 0.04 $mm^2$. The stress distribution of the square facilitates the stiffness of the structure which results in high resonant frequency. Therefore, this investigation shows that a high resonant frequency can be observed for the same area of rectangular PMUT.

## 4.7 Conclusion

In this chapter, the PMUT is analyzed layer-wise to observe the effect of critical design parameters on the resonant frequency. The critical design parameters such as radius and thickness are investigated comprehensively. In order to validate the authenticity of the COMSOL Multiphysics, the simulated values of the Step-I and Step-II are compared with the calculated values of the resonant frequency. The boundary conditions of the proposed designs are also discussed. Then, the proposed designs of PMUT with different shapes such as circle, square and rectangle are simulated by varying the radii. The radii are selected based on step I and II analyses as to design lower frequency devices. From the simulation analyses, the circular PMUT has a resonant frequency of 1.32 MHz for a radius of 115µm, the square PMUT has a resonant frequency of 1.95 MHz for an area of 0.04 $mm^2$ and the rectangular PMUT has a resonant frequency of 1.45 MHz for an area of 0.05 $mm^2$. The operating frequency of the proposed designs has been analyzed comprehensively. Thus, a PMUT working in lower frequency range is designed. The next chapter investigates the acoustic output pressure for each design when operated at their resonant frequencies.



www.manaraa.com

Furthermore, the effect of critical parameters on the acoustic output pressure is also investigated.



www.manaraa.com

# Chapter 5

# Critical Design Parameters and Acoustic Analyses of PMUT

*"Sound is the vocabulary of nature"*

*- Pierre Schaeffer*

## 5.1 Introduction

According to the first law of thermodynamics, "The energy can neither be created nor be destroyed." This law governs the transduction of any transducer system. The input electrical energy applied to the PMUT is converted to acoustic output energy [58]. The critical parameters such as radius, thickness, applied voltage, medium, distance are studied and evaluated to attain output pressure at the target frequency range. Moreover, to attain maximum output pressure, the PMUT must be operated at its natural vibrating frequency, the resonant frequency. As discussed in Chapter 4 and 6, the resonant frequency is determined for the proposed design. Therefore, the effect of output parameters such as radiation patterns of acoustic pressure and sound pressure level (SPL) in decibels are evaluated while operating at the resonant frequency of the respective designed geometries. In this chapter, the Acoustic module is coupled with the MEMS module under Multiphysics section to perform the acoustic analyses of the proposed PMUTs. Since the PMUT has asymmetric structure, the functionality such as 2D and 2D Axis symmetric modules has been utilized to execute the acoustic simulations. The boundary conditions, mesh settings along with extracted results are further discussed in this chapter.



www.manaraa.com

## 5.2 Acoustic Simulation Environment

As discussed in Chapter 4, the resonant frequency is determined for the proposed PMUT designs. In this section, the PMUTs are operated at their respective resonant frequencies. When an alternating voltage is applied to the PMUT, ultrasound is generated. The generated acoustic waves propagate through the tissues of the targeted area. Based on the acoustic impedance of the tissue, a portion of the signal is transmitted or reflected to the PMUT.

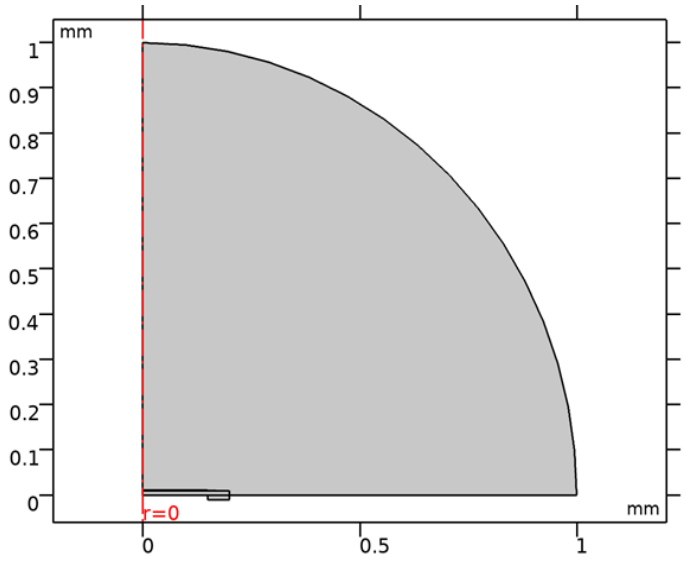


***Figure 27*** *A 2D axis-symmetric structure of the circular PMUT with a test medium domain of radius 1mm with a sector angle of 90º for the acoustic analyses.*

To simulate the acoustic output pressure of the proposed PMUT designs, the fabricated PMUT model has been simplified in COMSOL Multiphysics. The 2D component for rectangular PMUT and 2D axis-symmetric component for circular PMUT are selected to model the proposed structures. The active areas i.e. vibrating areas of the PMUTs are only considered for the simulation purposes. As shown in Figure 27, the simplified structure of PMUT for the acoustic analyses has a circle of radius 1mm with a sector angle of 90º. This circle is selected as the area for any test medium. This 2D component uses a “Revolution”



www.manaraa.com

functionality in the result sections to revolve the structure around the axis to give a 3D PMUT structure. As illustrated in Figure 28, a 2D component is utilized to design a single cell rectangular PMUT without the axis-symmetric functionality. The PMUT is placed at the center of the test domain of radius 1mm and 2mm with a sector angle of 180º.

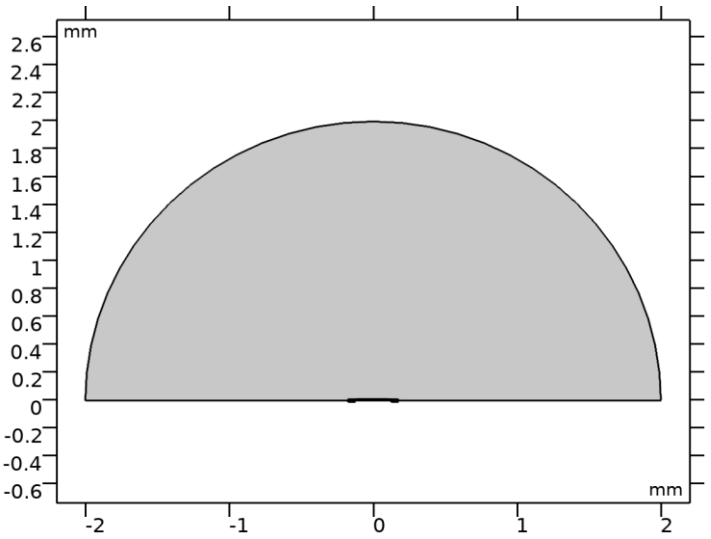


*Figure 28 A 2D structure of the rectangular PMUT with a test medium domain of radius 1mm with a sector angle of 180º for the acoustic analyses.*

The MEMS module which comprises of Electrostatics and Solid Mechanics is coupled with the Pressure Acoustic module of Frequency domain under the Multiphysics section. This acoustic module is utilized to analyze and evaluate the propagation of acoustic waves and their pressure variations in the selected test medium. A frequency domain study is conducted to analyze the effect on PMUT on applying a harmonic excitation of one frequency i.e. resonant frequency. The mesh element size, "Fine" is used under Physics-controlled mesh setting. As Figure 29 illustrates, the mesh is denser around the PMUT and less dense in the area of the medium.



www.manaraa.com

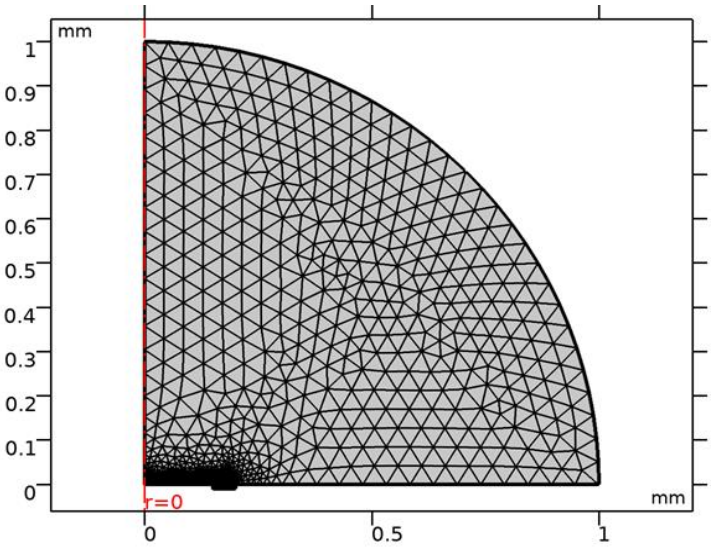


***Figure 29*** *The fine mesh setting of a 2D axis-symmetric circular PMUT*

As shown in Figure 30, for a fair comparison the same fine mesh setting is also selected to analyze the 2D rectangular PMUT. The mesh is denser for PMUT and less dense for the test domain.

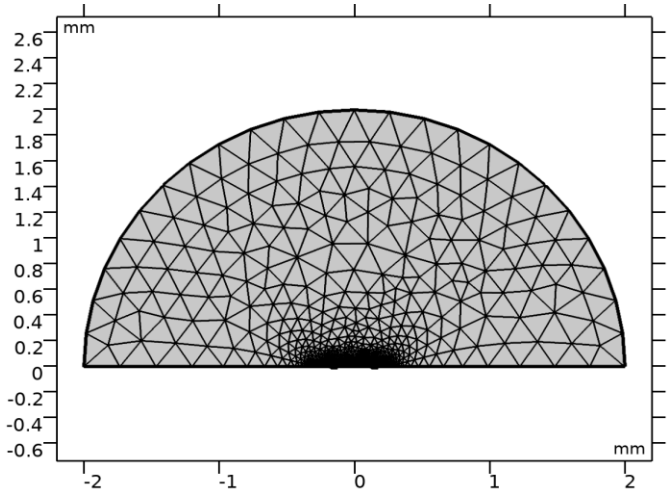


***Figure 30*** *The fine mesh setting of a 2D rectangular PMUT*

## 5.2.1 Boundary Conditions

The two proposed designs of 2D axis-symmetric circular PMUT and 2D rectangular PMUT are simulated for the acoustic analyses. As discussed in section 4.5.1 of Chapter 4,



www.manaraa.com

these designs are modelled based on the design rules of the PiezoMUMPs fabrication process. The parameters of the proposed circular and rectangular PMUT are listed in Table VIII.

***Table VIII*** *The parameters list such as radius, thickness and applied voltage for the proposed design, circular PMUT. The same parameters are used for rectangular and square PMUT by changing the radius.*

| Name of the parameter | Value[unit] | Description |
|---|---|---|
| $V_{ac}$ | 10, 20, 30, 40, 50 [V] | Applied AC voltage |
| r | 115, 170, 205, 250 [µm] | Range of varied radii of the piezo layer(AlN) |
| w | 250,300,350,400 [µm] | Range of the varied Width of the piezo layer of the rectangular PMUT |
| $r_{Al}$ or $w_{Al}$ | r-20 or w-20 [µm] | Radius or width of the top electrode (Al) |
| $r_{Si}$ or $w_{Si}$ | r+50 or w+50 [µm] | Radius or width of the Silicon substrate |
| $r_{SiO2}$ or $w_{SiO2}$ | r_Si-10 or w_Si-10 [µm] | Radius or width of Silicon dioxide |
| $t_{Al}$ | 1.02 [µm] | Thickness of the top electrode (Al) [Fixed] |
| $t_{AlN}$ | 500 [nm] | Thickness of the Aluminum Nitride [Fixed] |
| $t_{Si}$ | 10 [µm] | Thickness of the silicon substrate [Fixed] |
| $t_{Si}$ | 10 [µm] | Thickness of the silicon substrate [Fixed] |

The active areas such as silicon substrate, a bottom electrode, piezo layer and top electrode are simulated for both the circular and rectangular PMUT. The same boundary conditions



www.manaraa.com

as electrical analyses are followed here. However, the acoustic module has a different set of boundary conditions and each condition for both the designs are discussed in this section.

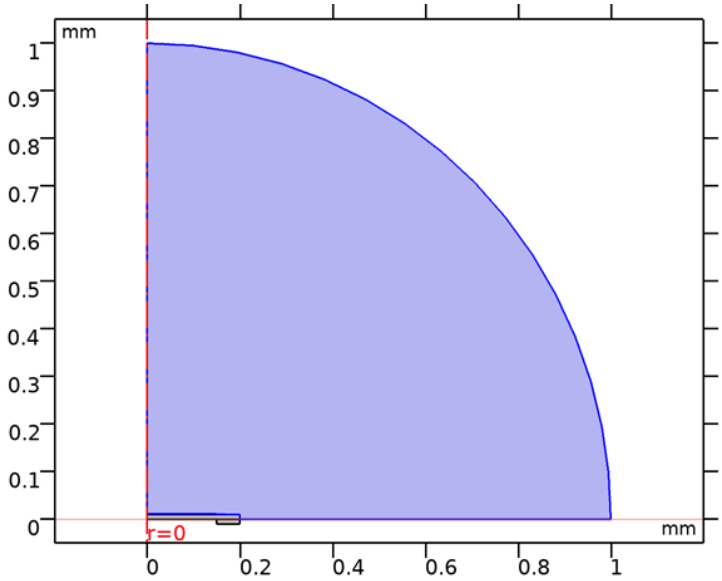


*Figure 31 The highlighted region is the selected domain for the pressure acoustics analyses for 2D axis-symmetric circular PMUT*

The pressure acoustics boundary condition for both the circular and rectangular PMUT are illustrated in Figures 31 and 32. The acoustic wave equation is given in Equation (10),

$$\nabla \cdot \left( -\frac{1}{\rho_c} (\nabla p_t - q_d) \right) - \frac{k_{eq}^2 p_t}{\rho_c} = Q_m \tag{10}$$

where $\rho$ is the density of the material, c is the speed of the sound, q and Q is the dipole and monopole domain sources respectively [69].

The entire circular domain of radius 1mm with a sector angle of 90º for the 2D component and 180º for 2D axis-symmetric component is selected to analyze the propagation of pressure waves.



www.manaraa.com

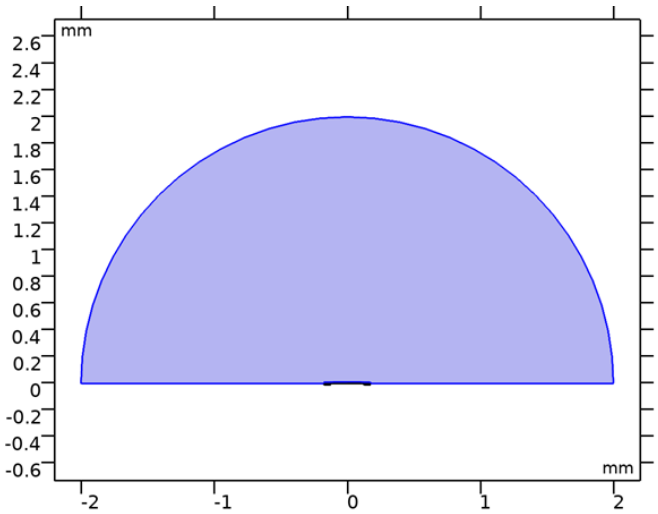


***Figure 32*** *The highlighted region is the selected domain for the pressure acoustics analyses for 2D rectangular PMUT.*

The sound hard boundary is a condition that makes the selected area to act as a wall by setting the normal component of the acceleration in the Equation (11) as zero. As shown in Figure 33, the region beside the PMUT is selected as sound hard boundaries [70].

$$-\mathrm{n}\cdot\left(-\frac{1}{\rho_c}(\nabla p_t - q_d)\right) = 0 \tag{11}$$

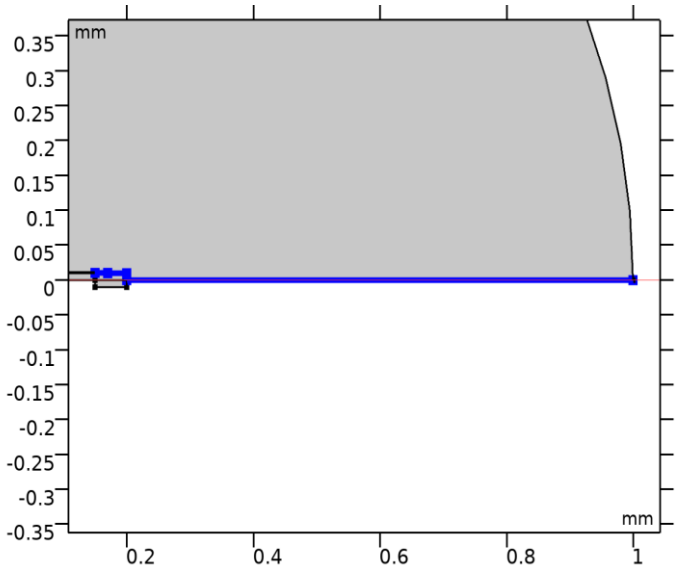


***Figure 33*** *The highlighted region is the selected domain for the sound hard boundary (wall) for 2D circular PMUT*



www.manaraa.com

As illustrated in Figure 34, the axial symmetry applies the symmetrical condition on the region r=0. The COMSOL rotates the structure at axis r=0.

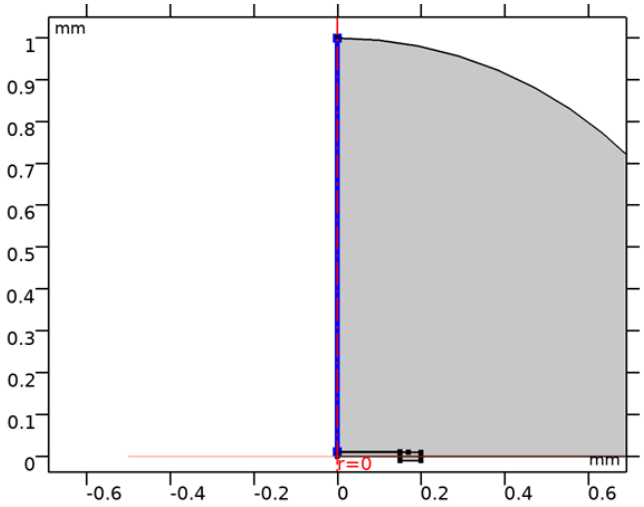


***Figure 34*** *Axial Symmetry condition of the 2D axis-symmetric circular PMUT.*

As shown in Figure 35, the spherical wave radiation condition is applied to the 2D axis-symmetric circular PMUT. This boundary condition allows the radiating ultrasound waves from the point $(x_0, y_0, z_0)$ to leave the domain and with minimum reflections at the boundary.

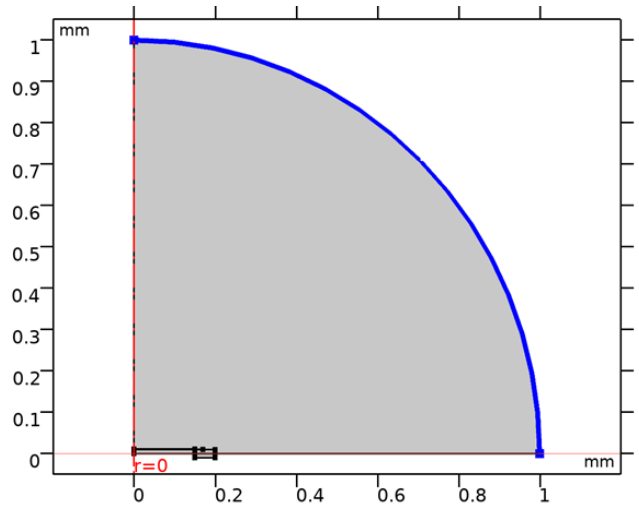


***Figure 35*** *Spherical Wave Radiation of a 2D axis-symmetric circular PMUT.*



www.manaraa.com

The governing equation is based on the spherical coordinates given by in Equation (12) [71],

$$-\mathrm{n}\cdot\left(-\frac{1}{\rho_c}(\nabla p_t - q_d)\right) + \left(ik_{eq} + \frac{1}{r_{rf}}\right)\frac{p}{\rho_c} - \frac{r_{rf}\Delta||p}{2\rho_c(1 + ik_{eq}r_{rf})} = Q_i \tag{12}$$

As shown in Figure 36, the cylindrical wave boundary condition is applied to the 2D rectangular PMUT. The radiating ultrasound is analyzed based on the cylindrical coordinates as shown in the Equation (13) and the field is assumed to be independent of the axis as this does not involve symmetrical condition.

$$-\mathrm{n}\cdot\left(-\frac{1}{\rho_c}(\nabla p_t - q_d)\right) + \left(ik_{eq} + \frac{1}{2r_{rf}} - \frac{1}{8r_{rf}(1 + ik_{eq}r_{rf})}\right)\frac{p}{\rho_c} - \frac{r_{rf}\Delta||p}{2(1 + ik_{eq}r_{rf})\rho_c} = Q_i \tag{13}$$

To evaluate the acoustic pressure outside the computational domain, COMSOL utilizes the Exterior Field Calculation. The analyses have been done using the Helmholtz-Kirchhoff equation, which is given in Equation (14) [71],

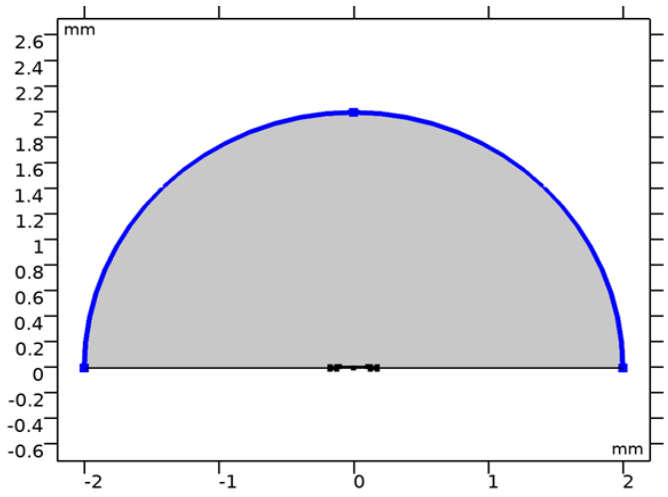


***Figure 36*** *Cylindrical Wave Radiation condition of 2D rectangular PMUT*



www.manaraa.com

$$p_{ext}(R) = \int_{S(r)}^{0} (G(R,r)\nabla p(r) - \nabla G(R,r)p(r) \cdot (-n)ds \tag{14}$$

The G(R, r) is the Green's Function where r is radiating wave from a source at R.

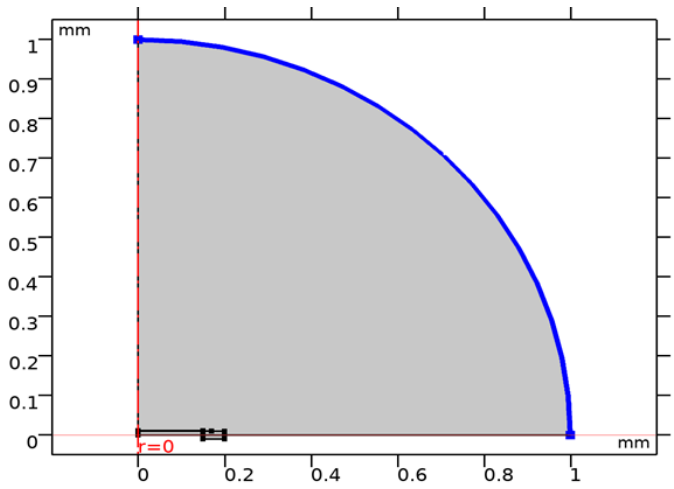


***Figure 37*** *Exterior Field Calculation boundary of the 2D axis-symmetric circular PMUT.*

As shown in Figure 37, the boundary of the circular domain is selected as the Exterior Field Calculation Boundary Condition. The results of this section are analyzed using the radiation pattern.

## 5.3 Effect of Radius

As the objective of the thesis is to generate acoustic output pressure using a low-frequency PMUT, the radius is varied to analyze and evaluate. Moreover, as discussed in Chapter 4, the PMUT is designed based on the PiezoMUMPs design rules so the thickness of the membranes cannot be varied. The dimensions of both the circular and rectangular PMUTs are converted to the area to perform a fair comparison as given in Table IX. The same dimensions and geometry, as listed in Table VIII, is selected for the analyses of the effect of thickness and medium on the acoustic output pressure for the proposed designs of the PMUT. As Figure 38 depicts, there is a decrease in the output pressure with the increase



www.manaraa.com

in the area of the piezo layer under the fixed biasing condition of 10 V. As discussed in 4.5.2 and 4.6.1, the smaller radii have the highest resonant frequency.

***Table IX*** *The geometries of the proposed PMUT with their respective area of the piezo layer*

| Geometry of the PMUT | Area of the Piezo layer ($mm^2$) |
|---|---|
| Circle | 0.04 |
| | 0.09 |
| | 0.13 |
| | 0.19 |
| Rectangle | 0.05 |
| | 0.06 |
| | 0.07 |
| | 0.08 |

The graphs in Figure 38 shows the maximum output pressure of 39.2 kPa at $0.04mm^2$ for the circular PMUT and 4.7 kPa at $0.05mm^2$ for the rectangular PMUT. This shows that the acoustic output pressure is inversely proportional to the area of the piezo layer under a fixed biasing condition.

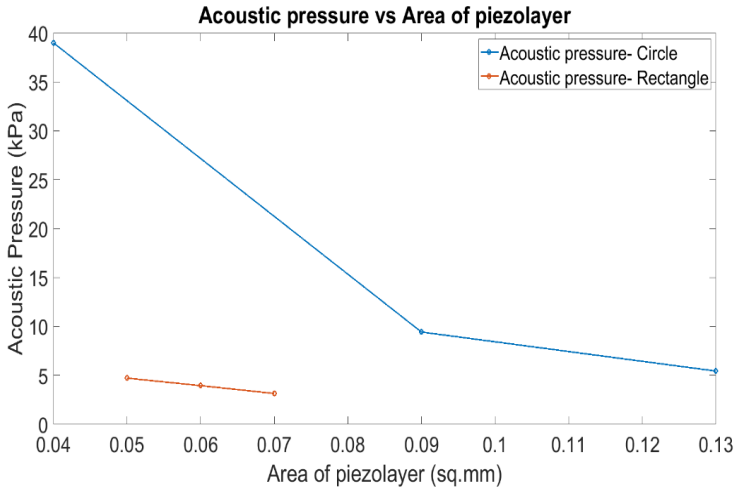


***Figure 38*** *This graph is plotted between the area of the piezo layer and the acoustic output pressure of both the circular and rectangular PMUT.*



www.manaraa.com

## 5.4 Effect of Voltage

To evaluate the effect of applied voltage on the acoustic output pressure, the voltage is varied from 10V to 20V for the proposed circular and rectangular PMUTs with dimensions listed in Table VIII. This voltage analyses have been done for both rectangular and circular PMUT. Both the designs are operated at their respective resonant frequencies.

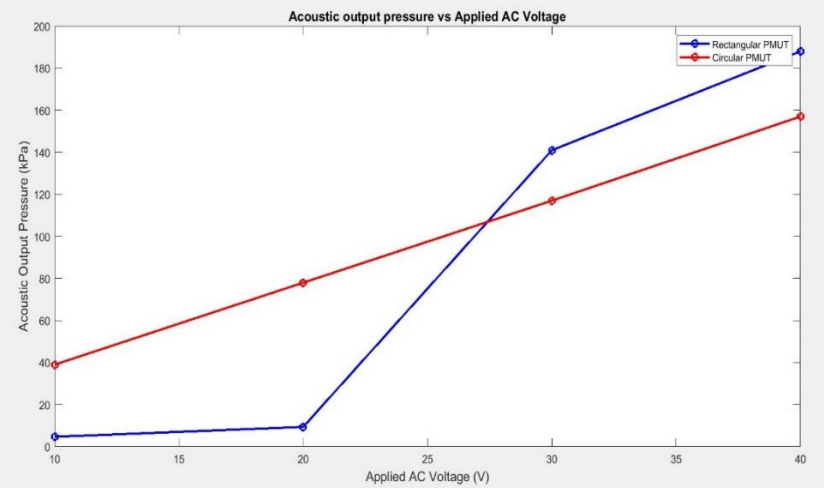


***Figure 39*** *This graph is plotted between the applied voltage and the acoustic output pressure of both the circular and rectangular PMUT.*

As shown in Figure 39, the acoustic pressure is directly proportional to the applied input voltage for a fixed active area. The pressure increases linearly for the circular PMUT whereas, for rectangular PMUT, it escalates after an input voltage of 20V. The circular PMUT of resonant frequency 1.32 MHz exhibits 39 kPa at 10V. A low voltage system also facilities a low power consuming system.

## 5.5 Effect of Medium

The tissues are made of a significant amount of water in their composition. Therefore, modelling waves in the liquid medium have been done to analyze and evaluate the effect of medium on the propagation of ultrasound. The speed of sound in water is



www.manaraa.com

specified as 1530 m/s throughout the analyses. The Total acoustic pressure field (Pa) analyses are done for both the circular and rectangular PMUTs in liquid and air medium. Moreover, the sound pressure level (dB), Exterior field pattern using radiation pattern are also evaluated for the proposed PMUT designs. The attenuation of the ultrasound concerning to distance is also evaluated in this section.

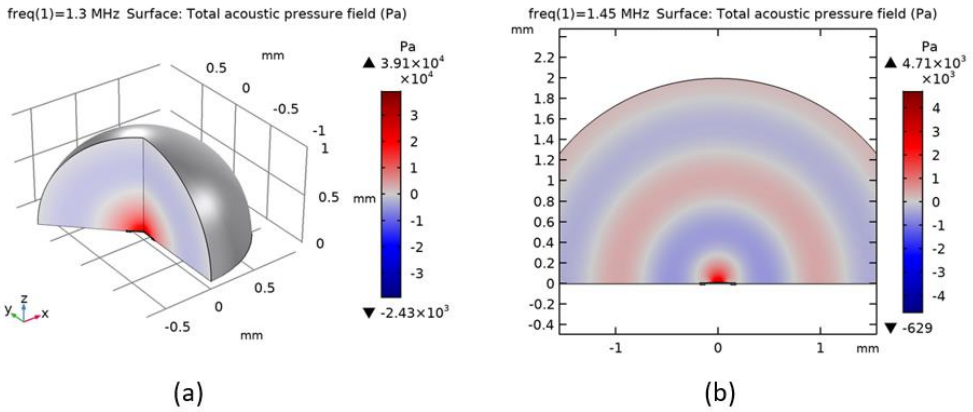


***Figure 40*** *Total acoustic pressure field analyses in 2D and 2D axis-symmetric components in the water medium. (a) 39.1 kPa is observed for the circular PMUT operated at its resonant frequency of 1.3 MHz for an input AC voltage of 10V. (b) 4.71 kPa is observed for the rectangular PMUT operated at its resonant frequency of 1.45 MHz for an input AC voltage of 10V.*

As illustrated in Figures 40(a) and 40(b), the acoustic pressure is higher at the center of PMUT creating a directional beam pattern. The rectangular PMUT provides 4.71 kPa for 10V. As depicted in Figure 38, the smallest area of both the designs delivered the higher output pressure under a fixed biasing condition. Figure 41 illustrates the decrease in the pressure level with an increase in the distance. A cut point functionality is used to evaluate the variation in pressure when the distance is increased. As illustrated in Figure 41(a), the cut point is plotted from point 0, center of the PMUT to the border of the 2mm water domain.



www.manaraa.com

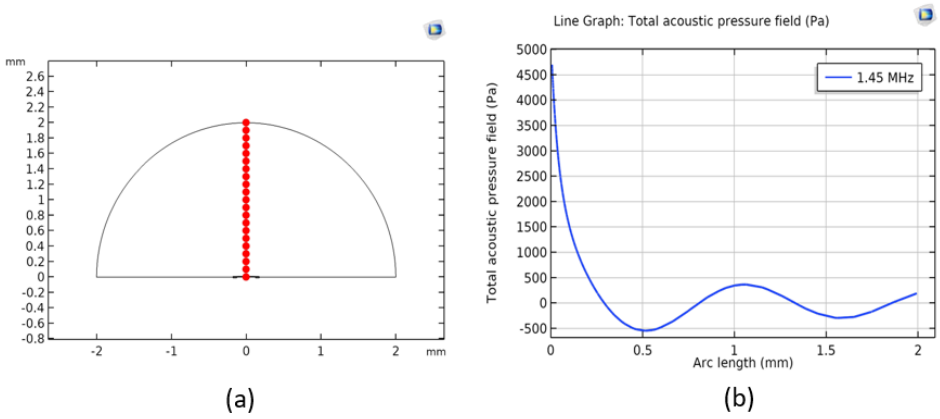


***Figure 41*** *(a) Cut-point of 2D rectangular PMUT. (b) The graph is plotted between the cut points vs acoustic pressure at that point.*

As shown in Figure 41(b), the amplitude of the ultrasound degrades as it moves further from the source due to attenuation, absorption of the energy by the tissues, scattering, reflection and refraction of the ultrasound by the heterogeneous mixture of the test medium. The 3D model of the propagation and attenuation of the acoustic output pressure is shown in Figure 40(b).

The next parameter, Sound Pressure level which measures the effective pressure of sound in terms of decibels (dB). It is calculated using the given formula:

$$SPL = 20\ \log_{10}\left(\frac{p}{p_0}\right)$$

Where SPL is sound pressure level, p is the sound pressure and $p_0$ is the reference sound pressure. The value of reference sound pressure is 20µPa. For instance, the total acoustic pressure level for circular PMUT as shown in Figure 40(a) is 3.91 kPa. Therefore, the value of p is 3.91 kPa and the value of $p_0$ is 20µPa. This gives the SPL for circular PMUT as 185 dB and the rectangular PMUT has a sound pressure level of 164 dB as shown in Figure 42(a) and 42(b). The radiation pattern of exterior field pressure evaluates the propagation



www.manaraa.com

of the ultrasound beam outside the computational domain as shown in Figure 43. The 2D radiation pattern evaluates the sense of direction of propagation of the ultrasound beam.

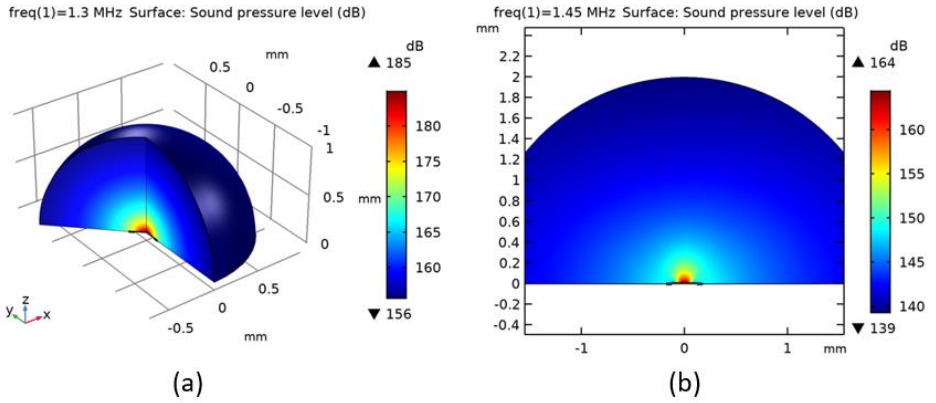


***Figure 42*** *Sound pressure level analyses in 2D and 2D axis-symmetric components in the water medium. (a) 185 dB is observed for the circular PMUT operated at its resonant frequency of 1.3 MHz for an input AC voltage of 10V. (b) 164 dB is observed for the rectangular PMUT operated at its resonant frequency of 1.45 MHz for 10V.*

As shown in Figure 43(a), the radiation pattern of the single cell circular PMUT is high directional in the water medium and no side lobes or grating lobes are observed. However, in rectangular PMUT, the main lobe is wider with no side or grating lobes. This shows that the directivity is higher in the proposed circular PMUT and the beam width is higher in the rectangular PMUT.

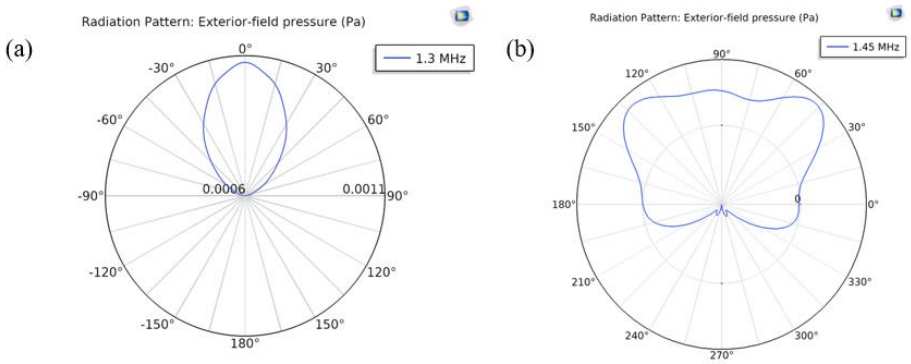


***Figure 43*** *The radiation pattern of exterior field pressure for (a) circular PMUT and (b) rectangular PMUT.*



www.manaraa.com

## 5.6 Conclusion

The acoustic analyses have been for the circular and the rectangular PMUT using COMSOL Multiphysics. The Pressure Acoustics module is coupled with the MEMS module to model the acoustic environment for the PMUT. In this chapter, a 2D component and 2D axis-symmetric components are employed to model the rectangular and circular PMUT respectively. The “Fine” mesh is used to both the designs to evaluate the acoustic output pressure. Followed by the boundary conditions of the acoustic model are discussed along with their respective governing equations. Furthermore, the critical parameters such as radius, applied voltage, distance and test medium are investigated thoroughly. The PMUTs are operated at their resonant frequency using the frequency domain study and the effect of radius, voltage and medium are studied. From the acoustic analyses, the circular PMUT exhibits 39.1 kPa when operated at its resonant frequency of 1.32 MHz for an input voltage of 10V. The radiation patterns of the circular PMUT shows higher directivity with no side or back lobes. The rectangular PMUT exhibits 4.7 kPa when operated at 1.45 MHz for an input voltage of 10V and has a wider beam width. Therefore, a low-frequency PMUT that can generate acoustic output pressure is designed and evaluated.



www.manaraa.com

# Chapter 6

# Proposed Designs and Electrical Characterization of PMUT

*"And on the eighth day God said, "Okay, Murphy, you're in charge."*

*– Author Unknown*

## 6.1 Introduction

The proposed PMUT device is fabricated using an advanced surface micromachining technique known as PiezoMUMPs. In this thesis, the proposed designs are designed and fabricated based on this PiezoMUMPs technique offered by MEMSCAP Inc. The PMUT chip is designed using MEMS Pro software. The fabrication steps of the proposed designs are discussed in detail in this chapter. Then the fabricated chip is tested to evaluate the resonant frequency of the individual PMUTs. The measured values are compared with the simulated values in the later section of this chapter.

## 6.2 PiezoMUMPs

The PiezoMUMPs is a piezoelectric micromachining process focusing on MEMS based piezoelectric devices. To achieve high yield, the dimensions and other critical parameters such as thickness, the order of material layers and the spacing are predetermined to accommodate all types of piezoelectric devices. This fabrication process has 5 mask layers. However, each layer has its pre-established values for thickness and material selections. The first layer starts with a doped silicon substrate. Thermal oxide is grown, patterned and etched. Followed by the deposition, patterning and etching of the piezo layer, Aluminum Nitride and the pad metal, chrome and aluminum. Then the silicon is lithographically patterned, and a protection layer is applied at the front side till the



www.manaraa.com

patterned silicon layer. Then the wafer is flipped, and the backside of the wafer is patterned and etched to create a trench. Finally, the protection layer is stripped off. The fabrication steps are discussed thoroughly in the next section [72].

### 6.2.1 Fabrication steps of the proposed PMUT

The fabrication is performed on a 150 nm n-type Silicon on Insulator (SOI) wafer. A phosphosilicate glass (PSG) layer is deposited on the silicon layer and annealed at 1050 ºC for one hour in Argon. The silicon layer is doped to increase electrical conductivity. Then the PSG layer is removed by a wet chemical etching process. This illustrated in Figure 44 [73].

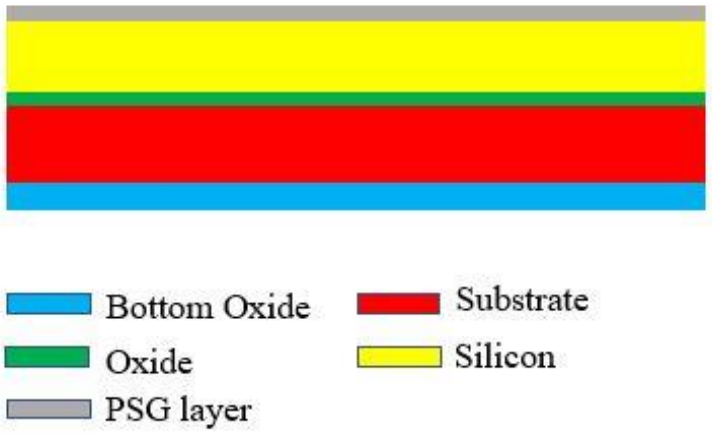


*Figure 44 Doping of silicon layer by Phosphosilicate glass layer on a 150 nm n-type Silicon on Insulator (SOI).*

After doping the silicon layer, a thermal oxide is grown of thickness 2000 Angstrom. Then the thermal oxide is coated with positive photoresist to create Pad Oxide. Photoresist, a material, sensitive to light used in the photolithography process to form patterns on layers. A positive photoresist is used as it becomes soluble when exposed to UV light. Therefore, the positive photoresist is lithographically patterned by the Pad Oxide Mask (First Level



www.manaraa.com

Mask). The remaining oxide is etched using the reactive ion etching process (RIE). The process is illustrated in Figure 45.

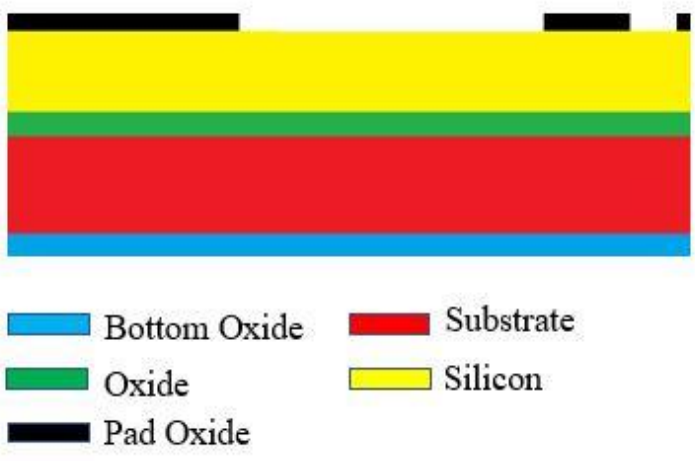


*Figure 45 The Pad Oxide is the first level masking. The pad oxide is grown 2000 Angstrom of thickness. It is then patterned lithographically and etched using RIE process.*

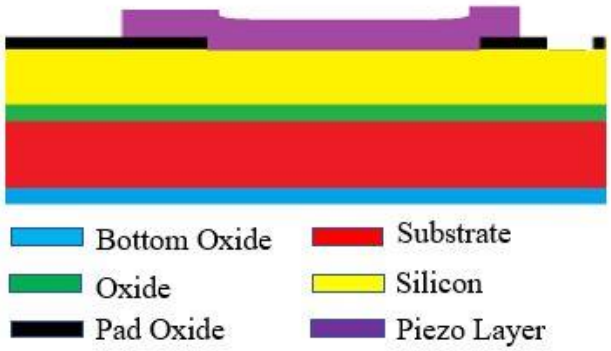


*Figure 46 Deposition of the piezo material is the second masking. A 0.5µm thickness of the piezo material is deposited using reactive sputtering. The piezo layer is lithographically patterned and wet etched.*

In this second level masking, a 0.5µm thickness of the piezo layer, Aluminum Nitride is deposited on the patterned thermal oxide by reactive sputtering. This method is selected as it provides control over the gas flow and preferred for thin film deposition. Then, the wafer is coated with positive photoresist. The second level mask is used to lithographically



www.manaraa.com

pattern the photoresist. Then, the remaining of the piezo film is wet etched. This is illustrated in Figure 46.

Followed by the deposition of the piezo layer, the pad metals are deposited. In this step, a negative photoresist is used to coat the wafer. The third level masking, pad metal, is used to lithographically pattern the photoresist. Then, a thickness of 20nm chrome and 1000nm aluminum is deposited using beam evaporation as shown in Figure 47. Then deep RIE etching is performed.

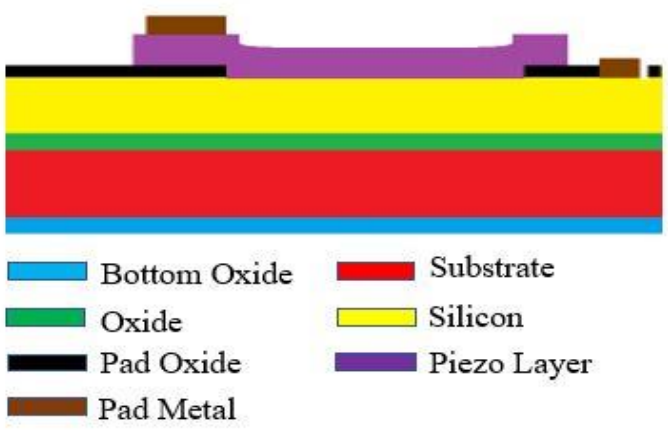


*Figure 47 Deposition of the pad metals is the third level masking. The negative photoresist is patterned and a 20nm chrome and 1000nm aluminum are deposited by beam evaporation.*

The fourth masking, SOI, is for lithographically patterning the silicon layer. As shown in Figure 48, the silicon is etched till the thermal oxide. At this stage, the wafer is coated with UV sensitive photoresist. Then the area is exposed to ultraviolet light which allows the patterned photoresist area to etch. The Inductively Coupled Plasma (ICP) is employed to perform the Deep RIE. This ICP technology mainly used to remove the remaining of the silicon.



www.manaraa.com

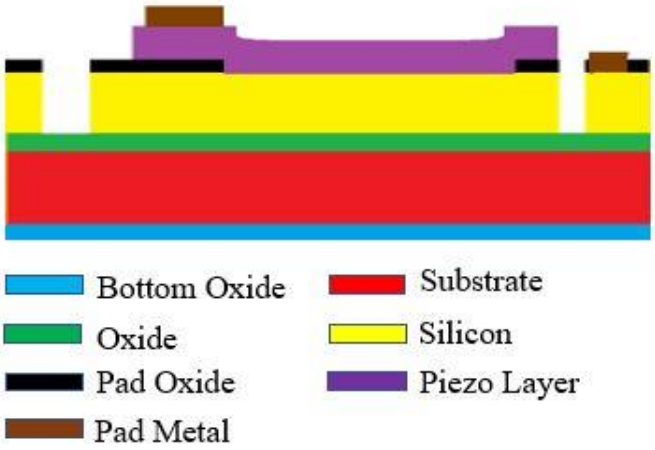


*Figure 48 Etching the silicon until the oxide layer using the fourth level masking, SOI. RIE and Deep RIE is used for the etching process. An UV sensitive photoresist is used to pattern the wafer*

The final process is to create a trench at the backside of the wafer. Therefore, a protective coating is applied at the front side of the wafer. As shown in Figure 49, a polyimide coating is used to hold the structure when the wafer is flipped. After the formation of the trench, the protective coating is removed using a dry etch process. In order to create a trench, the substrate is lithographically patterned using the fifth mask, Trench. Three etching process has been utilized to form the trench. Firstly, Reactive Ion Etching (RIE) is employed to etch the pattern into bottom oxide.

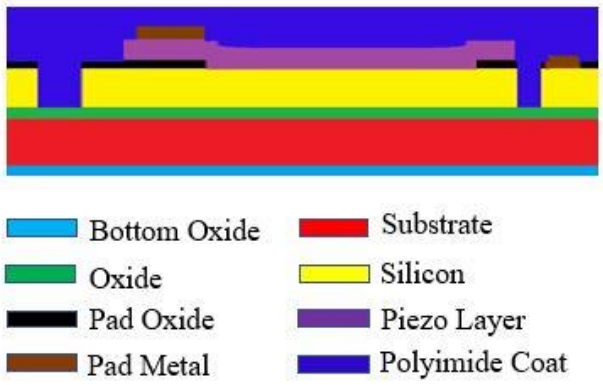


*Figure 49 A protection layer, polyimide coat is deposited at the front end of the wafer to hold the structure when the wafer is flipped to create the trench at the back end of the wafer.*



www.manaraa.com

Secondly, the substrate layer is etched using a DRIE silicon etching process. Lastly, the oxide layer above the substrate is etched using the wet oxide etch process. After the above-discussed process, the protection layer is removed, and the trench is created at the backside of the wafer. The process is illustrated in Figure 50.

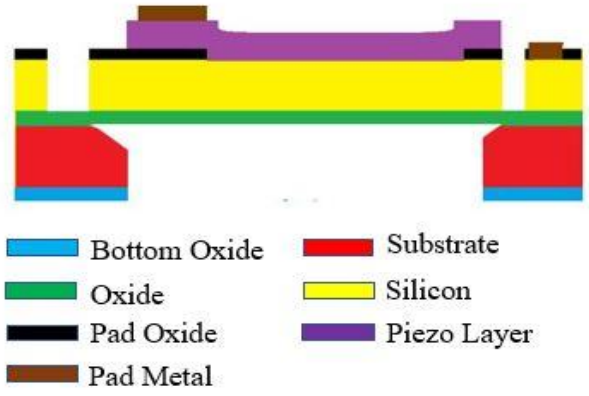


*Figure 50 Fifth mask level, Trench is used for patterning the substrate. RIE, DRIE Silicon etch and wet oxide etch processes are utilized to create the trench till the oxide layer.*

Hence, the PMUT is fabricated using a simple five-level masking fabrication process. The dies are then separated using a laser dicing technique. A CPGA209 is used to wire bond and package the chip.

## 6.2.2 Proposed PMUT Design and Fabricated Chip

The proposed PMUT designs as discussed in Chapter 4 is drawn as a layout in a chip using L-Edit MEMS Pro version-10. This software is used for design and analyses of MEMS devices. MEMS Pro has a functionality where the user can add the fabrication process as a layer palette. In this work, a PiezoMUMPs layer palette has been used to design the chip. As shown in Figure 51, different geometries such as circular, square and rectangular PMUTs has been arranged in the chip size of 4.5mm x 4.5mm to compare their



www.manaraa.com

resonant frequencies and power generation capabilities. The mechanical properties are given by the PiezoMUMPs design process which is listed in Table X.

***Table X*** *Layer names with their predetermined thickness of the PiezoMUMPs.*

| Layers in the PiezoMUMPs design process | Predetermined Thickness (µm) | |
|---|---|---|
| | Minimum | Maximum |
| Thermal Oxide | 0.195 | 0.21 |
| Substrate | 395 | 405 |
| Oxide | 0.95 | 1.05 |
| Silicon | 9 | 11 |
| Piezo Layer | - | 0.5 |
| Pad Metal | 0.47 | 1.02 |

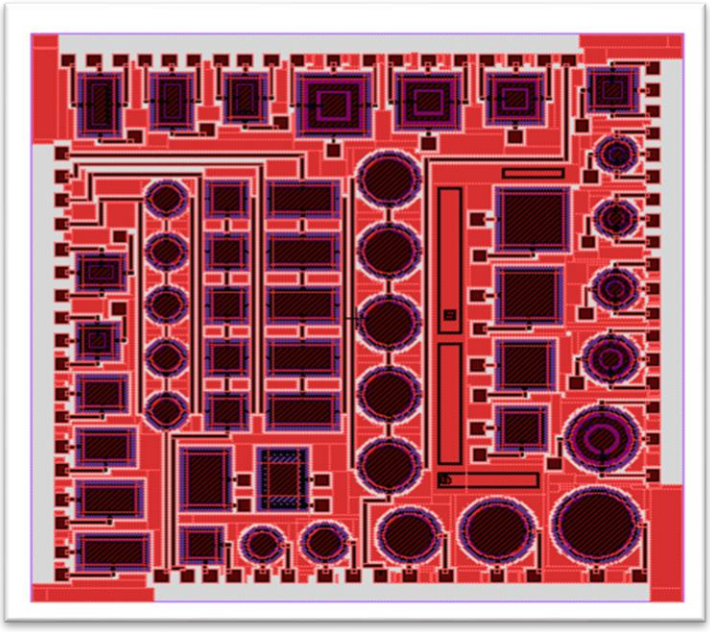

*Figure 51 Top view of the fabricated PMUT Chip – IMPWR001 in MEMS Pro using a standard PiezoMUMPs fabrication layer sequence.*



www.manaraa.com

As shown in Figure 51, the chip consists of individual PMUTs of different target geometries as designed in Chapter 4. The dimensions of the highlighted part in Figure 52 is listed in the table below.

***Table XI*** *The dimensions of the tested PMUT devices in the Chip – IMPWR001*

| Name of the PMUT geometries | Dimensions of the Piezo Layer (μm) |
|---|---|
| Circular PMUT (radius), 4 devices | 115, 170, 205, 250 |
| Square PMUT (side), 4 devices | 105, 115, 145, 205 |
| Rectangular PMUT (Width & Height), 4 devices | (250,200), (300,200), (350,200), (400,200) |

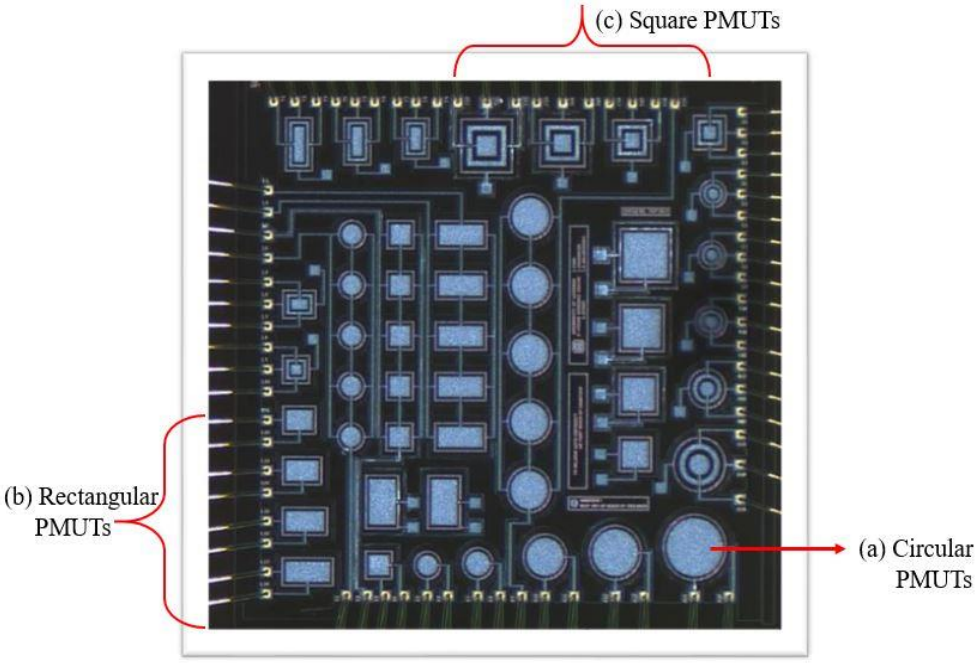


*Figure 52 The optical image of the fabricated PMUT chip – IMPWR001 (Top View). The highlighted parts are the geometries tested for analyses.*



www.manaraa.com

## 6.3 Electrical Characterization

To evaluate the properties of the fabricated devices, electrical characterization is performed using a Keysight Impedance Analyzer E4990A as shown in Figure 53. The measurement results are then compared with the simulation results presented in the previous chapters. This equipment is used to perform admittance-voltage measurements over the target frequency range. The probe voltage is set to 1V. The impedance measurements are done for the devices highlighted in Figure 52 with dimensions listed in Table XI.

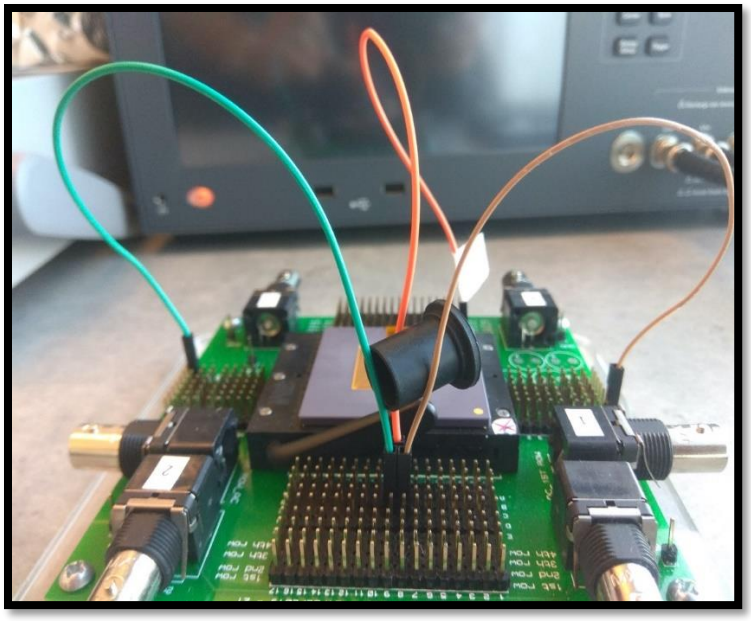

*Figure 53 Experimental test setup for the electrical characterization of PMUT chip – IMPWR001*

### 6.3.1 Simulation Verification

Electrical characterizations are conducted on the circular and rectangular designed PMUTs to validate the effect of the geometry on the device resonant frequencies at the target frequency range in this thesis. The measurement results are compared with the simulation results presented in the previous chapters, where the effects of device critical



www.manaraa.com

design parameters are investigated. To measure the resonant frequency in the impedance analyzer, a frequency sweep is conducted. Since the frequency range for this impedance analyzer is 20 Hz to 30 MHz, it can cover the low target frequency range of the devices designed in this work, designed to perform at lower than 3MHz. Unlike conventional PMUTs with higher than 10MHz operating frequency, the proposed PMUT designs are designed, modelled and optimized to operate at a frequency range of 0.5 MHz to 2 MHz. The electrical characterizations are performed at this frequency range. The start and end value in the fine sweep measurements are entered with an approximation value lesser than 0.5 MHz. For instance, the simulated value for a circular PMUT of radius 170µm is 0.748 MHz. Therefore, the frequency ranges with a start value of 0.5 MHz and an end value of 0.9 MHz is set in the impedance analyzer. The same procedure is followed for all the evaluated devices. In this particular device, after the sweep, the resonant frequency is identified at 0.731 MHz. The entire process is repeated for the entire devices in the PMUT chip. As shown in Table XII, the measured resonant frequencies are compared with the simulated resonant frequencies with their deviation expressed in MHz and plotted in Figure 54.

***Table XII*** *Comparison of resonant frequencies of proposed PMUTs with their deviation.*

| Geometry of the PMUT | Area of the PMUT ($mm^{2)}$ | Simulated Resonant Frequency (MHz) | Measured Resonant Frequency (MHz) | Deviation Value (MHz) | Error (%) |
|---|---|---|---|---|---|
| Circular PMUT | 0.04 | 1.32 | 1.86 | 0.54 | 40.9 |
| | 0.09 | 0.74 | 0.73 | 0.01 | 1.3 |
| | 0.13 | 0.55 | 0.48 | 0.07 | 12.7 |
| | 0.19 | 0.4 | 0.3 | 0.1 | 25 |
| Rectangular PMUT | 0.05 | 1.45 | 1.58 | 0.13 | 8.9 |
| | 0.06 | 1.34 | 1.34 | 0 | 0 |
| | 0.07 | 1.27 | 1.18 | 0.09 | 7 |
| | 0.08 | 1.22 | 1.07 | 0.15 | 12.2 |



www.manaraa.com

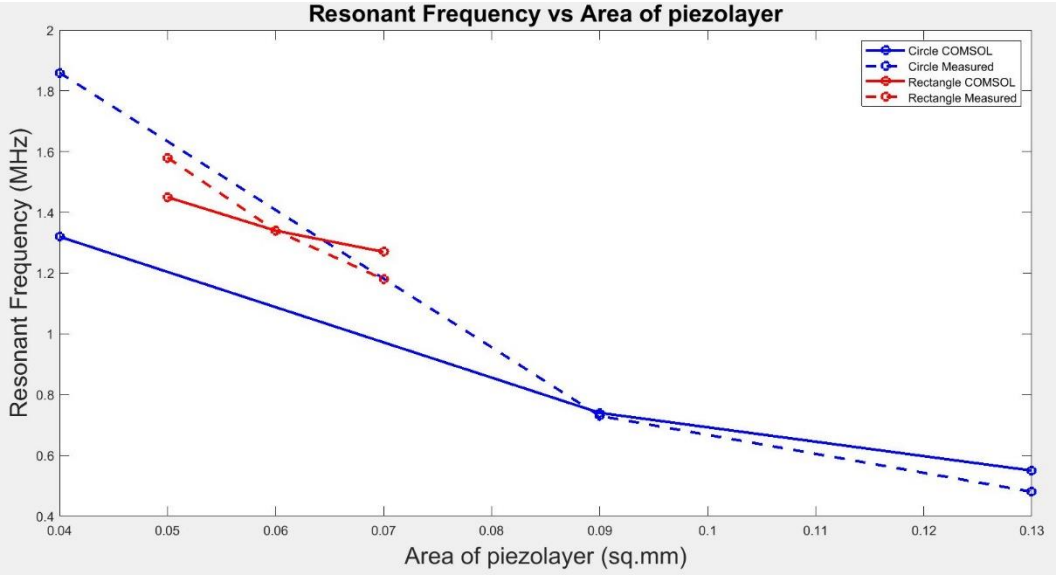


*Figure 54 The graph is plotted for measured and simulated values of resonant frequencies of the PMUT versus the area of the piezo layer of each geometry of the proposed PMUT designs.*

Figure 54 depicts that the extracted resonant frequency values from the impedance analyzer agree well with the FEM results which are discussed in Chapter 4. As the thickness of the layers is predetermined by the PiezoMUMPs design rules, the radius, side, width and height of the different geometries are converted to an area for a fair comparison. For instance, the circular PMUT with 115µm radius, a resonant frequency of 1.86 MHz is measured. The simulated resonant frequency for this device where the anchors and substrate were ignored in the simulations is 1.32 MHz which matches closely with the measurement result, validating the design methodology to develop the low frequency circular PMUT. The same procedure has been used for measuring the rest of the fabricated circular PMUTs. For the figure of merit, the rectangular PMUTs has been designed and verified with the aforementioned measurement procedure. For instance, the rectangular PMUT with width 250µm and height 200µm has a measured resonant frequency of 1.58 MHz and a simulated frequency of 1.45 MHz. This 0.13 MHz difference in the measured and simulated resonant frequency is due to the consideration of active areas in the PMUT for simulation purposes



www.manaraa.com

and systematic errors in the measurement. Moreover, the graph validates the authenticity and efficiency of the COMSOL Multiphysics software.

## 6.4 Conclusion

In this chapter, the proposed PMUT designs are developed using the PiezoMUMPs fabrication process. The step by step process of the fabrication is discussed. As this technique provides a cost-effective fabrication, it is utilized in this thesis. The proposed designs of the PMUT are drawn and analyzed using the MEMS Pro software. Furthermore, the fabricated PMUT chip – IMPWR001 is tested i.e. electrical characterization is performed using the impedance analyzer. After extracting the measured resonant frequency values, it is compared with simulated values from COMSOL Multiphysics. The graph in Figure 54 shows that the measured values agree well with the FEA results. Therefore, the operating resonant frequency for each PMUT in the proposed designs is validated. The following process is to operate the PMUT at the validated resonant frequency to determine the acoustic output pressure accordingly.



www.manaraa.com

# Chapter 7

# Conclusion and Future Work

*"The journey of a thousand miles begins with one step. "*

*-Lao Tzu*

Early detection of breast cancer prevents further development of the cancerous tissues and provides a significant amount of time for the doctors to arrange the appropriate treatments. The breast is mostly made of fat tissues. It also has the blood vessels, ducts and lobules which are the deeper tissues. The depth of the common axillary lymph nodes is between 1.4cm to 8cm [74]. Therefore, identifying the deeper cancerous tissues in the breast requires an appropriate imaging device to perform the early detection. The implementation of advanced micro and nanotechnology in the field of medical imaging devices increased the possibility of developing cost-effective portable devices. Piezoelectric Micromachined Ultrasound Transducer (PMUT) is a MEMS based transducer which has gained the attention of the researchers to develop with aforementioned configurations. Unlike conventional ultrasound transducer, the structure of PMUT is simple which facilitates the batch fabrication. In common, medical imaging systems utilize higher frequency for working operations. A high-frequency ultrasound transducer offers better resultant images and resolution. However, it has a higher attenuation rate as the frequency is directly proportional to the rate of attenuation of the signal [75]. The selection of the frequency range is based on the application. In some cases, to reach the deeper organs or tissues, a lower-frequency signal is required. In an effort to develop a lower-frequency PMUT, the critical design parameters such as radius, the



www.manaraa.com

thickness of the membrane, material properties of each layer are studied, analyzed and evaluated. Also, the design parameters influencing on the acoustic output pressure such as test medium, geometry are studied and evaluated. The proposed designs of PMUT are analyzed, simulated and fabricated to determine the appropriate resonant frequency and respective acoustic output pressure.

## 7.1 Summary and Conclusion

In this thesis, a low-frequency PMUT with measurable acoustic output pressure, a proof of concept, is developed. To understand and analyze the working mechanism of PMUT, the fundamental structure with the governing equations are studied. The effect of piezoelectricity along with the equivalent circuit model is investigated to discern the underlying theory of electromechanical coupling. FEA simulations are conducted using COMSOL Multiphysics to design a PMUT which operates at lower frequencies and to provide better acoustic performance. Kazari et al [76] designed lower frequency PMUTs using PiezoMUMPs. They designed, characterized and tested a circular and octagonal PMUTs for non-destructive testing in solids. They tuned their PMUTs to operate at 1MHz, 1.5MHz and 2MHz for higher-harmonics based nonlinear ultrasonic testing.

Firstly, the resonant frequency is determined for each of the proposed PMUT designs by performing an electrical analysis. To examine the structure, layer by layer analyses has been done by altering the critical design parameters such as radius, thickness. The Step I analyses, the piezo layer is simulated first and the results show that smaller radius and thicker membrane contributes higher resonant frequency. As the mechanical motion of the device determines the operating frequency, the effect of the addition of the silicon substrate to the piezo layer, Step II, is investigated. A similar trend is discerned that the radius is



www.manaraa.com

inversely proportional, and the thickness is directly proportional to the resonant frequency. Analytical modelling has been done to calculate the resonant frequency. The calculated and simulated values for both the Step I and Step II are compared to study the deviations. The calculated values of the Step I agree well with the simulated values. However, in Step II, the equation does not hold for a multi-layered structure. Therefore, COMSOL Multiphysics is employed to perform both the electrical and acoustic analyses of the multi-layered structure, PMUT.

The investigation of the proposed PMUT designs such as Circular, Square and Rectangular is done by investigating, analyzing, and evaluating the critical parameters. The proposed designs are based on the rules given by the PiezoMUMPs fabrication process where the thickness of each layer as well as structural materials are predetermined. Three low-frequency designed are proposed and the simulation results show that the resonant frequency of the circular PMUT is 1.3 MHz, the square PMUT has 1.9 MHz and the rectangular PMUT has 1.45 MHz. Thus, lower frequency PMUTs are developed. Furthermore, the proposed PMUT design layers are developed. The required mask layers of all the proposed designs are drawn using MEMS Pro software and then fabricated using PiezoMUMPs fabrication process. The fabricated prototype chip – IMPWR001 is tested by performing electrical characterizations using an impedance analyzer. The electrical characterizations show that the measure resonant frequency agrees well with the simulation results. Thus, the resonant frequency is determined for each low-frequency PMUT designs.

Based on the electrical analyses and characterizations, the acoustic analyses are performed for circular and rectangular PMUTs using COMSOL simulations. Each PMUT is operated at their respective resonant frequencies to achieve the maximum output



www.manaraa.com

pressure. The acoustic simulation environment with the governing equations is investigated. The critical parameters such as radius, applied input AC voltage, test medium is varied to investigate their effects on acoustic output pressure. The acoustic analyses results show that the circular PMUT presents 39.1 kPa at 1.32 MHz and the rectangular PMUT exhibits 4.7 kPa when operated at 1.45 MHz for a low input voltage of 10V. The radiation patterns of the circular PMUT shows higher directivity and rectangular PMUT with wider beam width with no side or grating lobes. Thus, a low-frequency PMUT with high acoustic output pressure is developed.

## 7.2 Future Work

The fabricated PMUT chip in this thesis consists of individual PMUT with different geometries. An array structure for each geometry needs to be studied, modelled, investigated and fabricated. A separate study on array arrangement needs to be done to analyze the cross-talking effects. The fabricated chip with array structures has to be tested by performing an acoustic characterization to further enhance the acoustic output performance. Moreover, the test results facilitate the improvement on the propagation of ultrasound, bandwidth and quality factor.



www.manaraa.com

# REFERENCES/BIBLIOGRAPHY


[1] "Breast cancer statistics 2020," Accessed on: June 15,2020. [Online]. Available:https://www.cancer.ca/en/cancerinformation/cancertype/breast/statistics/?region=on.

[2] J. Rouyer, S. Mensah, E. Franceschini, P. Lasaygues, and J.-P. Lefebvre, "Conformal ultrasound imaging system for anatomical breast inspection," *IEEE Trans. Ultrason. Ferroelectr. Freq. Control*, vol. 59, no. 7, pp. 1457–1469, Jul. 2012, doi: 10.1109/TUFFC.2012.2346.

[3] *MEMS Technology for Biomedical Imaging Applications*. MDPI - Multidisciplinary Digital Publishing Institute, 2019.

[4] D. Berger, "A brief history of medical diagnosis and the birth of the clinical laboratory. Part 1--Ancient times through the 19th century," *MLO. Med. Lab. Obs.*, vol. 31, no. 7, pp. 28–30, 32, 34–40, Jul. 1999.

[5] W. G. Bradley, "History of Medical Imaging," *Proc. Am. Philos. Soc.*, vol. 152, no. 3, pp. 349–361, 2008.

[6] A. Katsevich, "Theoretically Exact Filtered Backprojection-Type Inversion Algorithm for Spiral CT," *SIAM J. Appl. Math.*, vol. 62, no. 6, pp. 2012–2026, Jan. 2002, doi: 10.1137/S0036139901387186.

[7] J. T. Bushberg, *The essential physics of medical imaging*. Philadelphia, PA: Wolters Kluwer / Lippincott Williams & Wilkins, 2012.

[8] S. Gondrom, J. Zhou, M. Maisl, H. Reiter, M. Kröning, and W. Arnold, "X-ray computed laminography: an approach of computed tomography for applications with limited access," *Nucl. Eng. Des.*, vol. 190, no. 1, pp. 141–147, Jun. 1999, doi: 10.1016/S0029-5493(98)00319-7.

[9] G. M. Ardran, "The Application and Limitation of the Use of X-Rays in Medical Diagnosis," *Philos. Trans. R. Soc. Lond. Ser. Math. Phys. Sci.*, vol. 292, no. 1390, pp. 147–156, 1979.

[10] B. L. Zaret, *The patient's guide to medical tests*. Boston: Houghton Mifflin Co, 1997.

[11] E. Whaites, "Essentials of Dental Radiography and Radiology," p. 26.




المنارة للاستشارات
www.manaraa.com

[12] D. J. Brenner and E. J. Hall, “Computed Tomography — An Increasing Source of Radiation Exposure,” *N. Engl. J. Med.*, vol. 357, no. 22, pp. 2277–2284, Nov. 2007, doi: 10.1056/NEJMra072149.

[13] A. D. Sweeney, M. L. Carlson, A. Rivas, M. L. Bennett, D. S. Haynes, and G. B. Wanna, “The limitations of computed tomography in adult cochlear implant evaluation,” *Am. J. Otolaryngol.*, vol. 35, no. 3, pp. 396–399, Jun. 2014, doi: 10.1016/j.amjoto.2014.03.002.

[14] Cherry, Simon R., James A. Sorenson, and Michael E. Phelps, *Physics in nuclear medicine e-Book*. . Elsevier Health Sciences, 2012.

[15] C. M. Minderovic, “Nuclear Medicine,” in *The Gale Encyclopedia of Science*, 5th ed., vol. 6, K. L. Lerner and B. W. Lerner, Eds. Farmington Hills, MI: Gale, 2014, pp. 3067–3069.

[16] R. S. of N. A. (RSNA) and A. C. of Radiology (ACR), “Nuclear Medicine, General.” https://www.radiologyinfo.org/en/info.cfm?pg=gennuclear (accessed Jul. 15, 2020).

[17] H. H. Mitchell, T. S. Hamilton, F. R. Steggerda, and H. W. Bean, “THE CHEMICAL COMPOSITION OF THE ADULT HUMAN BODY AND ITS BEARING ON THE BIOCHEMISTRY OF GROWTH,” 1945.

[18] L. P. Clarke *et al.*, “MRI segmentation: Methods and applications,” *Magn. Reson. Imaging*, vol. 13, no. 3, pp. 343–368, Jan. 1995, doi: 10.1016/0730-725X(94)00124-L.

[19] G. Schultz, “Physical and Technical Background,” in *Magnetic Resonance Imaging with Nonlinear Gradient Fields: Signal Encoding and Image Reconstruction*, G. Schultz, Ed. Wiesbaden: Springer Fachmedien Wiesbaden, 2013, pp. 11–38.

[20] D. J. Grand, *Practical body MRI protocols, applications, and image interpretation*. Cambridge ; Cambridge University Press, 2012.

[21] G. Horga, T. Kaur, and B. S. Peterson, “Annual Research Review: Current limitations and future directions in MRI studies of child- and adult-onset developmental psychopathologies,” *J. Child Psychol. Psychiatry*, vol. 55, no. 6, pp. 659–680, Jun. 2014, doi: 10.1111/jcpp.12185.

[22] S. H. Faro and F. B. Mohamed, *Functional MRI Basic Principles and Clinical Applications*, 1st ed. 2006. New York, NY: Springer New York, 2006.



www.manaraa.com

[23] R. M. Nally, "Ultrasound Imaging," in *Handbook of Visual Display Technology*, J. Chen, W. Cranton, and M. Fihn, Eds. Berlin, Heidelberg: Springer, 2012, pp. 373–383.

[24] A. Almufleh, P. Di Santo, and J. A. Marbach, "Training Cardiology Fellows in Focused Cardiac Ultrasound," *J. Am. Coll. Cardiol.*, vol. 73, no. 9, pp. 1097–1100, Mar. 2019, doi: 10.1016/j.jacc.2019.01.027.

[25] M. Sibal, *Ultrasound in Gynecology: An Atlas and Guide*. Singapore: Springer Singapore, 2017.

[26] H. H. T. Madsen and F. Rasmussen, "Contrast-enhanced ultrasound in oncology," *Cancer Imaging*, vol. 11 Spec No A, no. 1A, pp. S167–S173, 2011, doi: 10.1102/1470-7330.2011.9042.

[27] D. Maulik, *Doppler Ultrasound in Obstetrics and Gynecology*, 2nd ed. Berlin, Heidelberg: Springer Berlin Heidelberg, 2005.

[28] J. S. Abramowicz, "Ultrasound in Reproductive Medicine: Is It Safe?," in *Ultrasound Imaging in Reproductive Medicine: Advances in Infertility Work-up, Treatment and ART*, L. A. Stadtmauer and I. Tur-Kaspa, Eds. Cham: Springer International Publishing, 2019, pp. 3–17.

[29] C. R. Porter and E. M. Wolff, *Prostate Ultrasound Current Practice and Future Directions*, 1st ed. 2015. New York, NY: Springer New York, 2015.

[30] H. Azhari, *Basics of biomedical ultrasound for engineers*. Hoboken, New Jersey: Wiley, 2010.

[31] L. W. Schmerr Jr, *Ultrasonic Nondestructive Evaluation Systems Models and Measurements*, 1st ed. 2007. New York, NY: Springer US, 2007.

[32] J. A. Gallego-Juarez, G. Rodriguez-Corral, and L. Gaete-Garreton, "An ultrasonic transducer for high power applications in gases," *Ultrasonics*, vol. 16, no. 6, pp. 267–271, Nov. 1978, doi: 10.1016/0041-624X(78)90053-7.

[33] R. S. C. Cobbold, *Foundations of Biomedical Ultrasound*. Oxford University Press, 2006.

[34] S. Abbas Shobeiri, "2D/3D Endovaginal and Endoanal Instrumentation and Techniques," in *Practical Pelvic Floor Ultrasonography: A Multicompartmental Approach to 2D/3D/4D Ultrasonography of the Pelvic Floor*, S. A. Shobeiri, Ed. Cham: Springer International Publishing, 2017, pp. 23–48.



www.manaraa.com

[35] K. Shung, "The Principle of Multidimensional Arrays," *Eur. J. Echocardiogr.*, vol. 3, no. 2, pp. 149–153, Jun. 2002, doi: 10.1053/euje.2001.0139.

[36] Q. Zhou, K. H. Lam, H. Zheng, W. Qiu, and K. K. Shung, "Piezoelectric single crystal ultrasonic transducers for biomedical applications," *Prog. Mater. Sci.*, vol. 66, pp. 87–111, Oct. 2014, doi: 10.1016/j.pmatsci.2014.06.001.

[37] B. Dubus, J. C. Debus, J. N. Decarpigny, and D. Boucher, "Analysis of mechanical limitations of high power piezoelectric transducers using finite element modelling," *Ultrasonics*, vol. 29, no. 3, pp. 201–207, May 1991, doi: 10.1016/0041-624X(91)90057-F.

[38] N. Aurelle, D. Guyomar, C. Richard, P. Gonnard, and L. Eyraud, "Nonlinear behavior of an ultrasonic transducer," *Ultrasonics*, vol. 34, no. 2, pp. 187–191, Jun. 1996, doi: 10.1016/0041-624X(95)00077-G.

[39] T. R. Gururaja, W. A. Schulze, L. E. Cross, R. E. Newnham, B. A. Auld, and Y. J. Wang, "Piezoelectric Composite Materials for Ultrasonic Transducer Applications. Part I: Resonant Modes of Vibration of PZT Rod-Polymer Composites," *IEEE Trans. Sonics Ultrason.*, vol. 32, no. 4, pp. 481–498, Jul. 1985, doi: 10.1109/T-SU.1985.31623.

[40] "An Introduction to MEMS (Micro-electromechanical Systems)," p. 56, 2002.

[41] INSPEC and T.-R. Hsu, *MEMS packaging*. London: INSPEC, 2004.

[42] R. Ghodssi and P. Lin, *MEMS Materials and Processes Handbook*, 1st ed. New York, NY: Springer US, 2011.

[43] B. T. Khuri-Yakub, Y. Huang, and A. S. Ergun, "Micromachined ultrasonic transducers and method of fabrication," US6958255B2, Oct. 25, 2005.

[44] S. Tadigadapa and K. Mateti, "Piezoelectric MEMS sensors: state-of-the-art and perspectives," *Meas. Sci. Technol.*, vol. 20, no. 9, p. 092001, Jul. 2009, doi: 10.1088/0957-0233/20/9/092001.

[45] O. Oralkan *et al.*, "Capacitive micromachined ultrasonic transducers: next-generation arrays for acoustic imaging?," *IEEE Trans. Ultrason. Ferroelectr. Freq. Control*, vol. 49, no. 11, pp. 1596–1610, Nov. 2002, doi: 10.1109/TUFFC.2002.1049742.



www.manaraa.com

[46] B. T. Khuri-Yakub and Ö. Oralkan, "Capacitive micromachined ultrasonic transducers for medical imaging and therapy," *J. Micromechanics Microengineering*, vol. 21, no. 5, p. 054004, Apr. 2011, doi: 10.1088/0960-1317/21/5/054004.

[47] A. S. Erguri, Yongli Huang, Xuefeng Zhuang, O. Oralkan, G. G. Yarahoglu, and B. T. Khuri-Yakub, "Capacitive micromachined ultrasonic transducers: fabrication technology," *IEEE Trans. Ultrason. Ferroelectr. Freq. Control*, vol. 52, no. 12, pp. 2242–2258, Dec. 2005, doi: 10.1109/TUFFC.2005.1563267.

[48] O. Onen and R. Guldiken, "Detailed investigation of capacitive micromachined ultrasonic transducer design space," *Microsyst. Technol.*, vol. 18, no. 4, pp. 399–408, Apr. 2012, doi: 10.1007/s00542-012-1449-5.

[49] A. S. Ergun, G. G. Yaralioglu, and B. T. Khuri-Yakub, "Capacitive Micromachined Ultrasonic Transducers: Theory and Technology," *J. Aerosp. Eng.*, vol. 16, no. 2, pp. 76–84, Apr. 2003, doi: 10.1061/(ASCE)0893-1321(2003)16:2(76).

[50] K. Smyth, S. Bathurst, F. Sammoura, and S.-G. Kim, "Analytic solution for N-electrode actuated piezoelectric disk with application to piezoelectric micromachined ultrasonic transducers," *IEEE Trans. Ultrason. Ferroelectr. Freq. Control*, vol. 60, no. 8, pp. 1756–1767, Aug. 2013, doi: 10.1109/TUFFC.2013.2756.

[51] F. Akasheh, T. Myers, J. D. Fraser, S. Bose, and A. Bandyopadhyay, "Development of piezoelectric micromachined ultrasonic transducers," *Sens. Actuators Phys.*, vol. 111, no. 2, pp. 275–287, Mar. 2004, doi: 10.1016/j.sna.2003.11.022.

[52] H. CHOI, "FABRICATION, CHARACTERIZATION AND MODELING OF K31 PIEZOELECTRIC MICROMACHINED ULTRASONIC TRANSDUCERS (pMUTs)," WASHINGTON STATE UNIVERSITY, 2007.

[53] A. B. Amar, H. Cao, and A. B. Kouki, "Modeling and process design optimization of a piezoelectric micromachined ultrasonic transducers (PMUT) using lumped elements parameters," *Microsyst. Technol.*, vol. 23, no. 10, pp. 4659–4669, Oct. 2017, doi: 10.1007/s00542-016-3205-8.

[54] S. Alasatri, L. Rufer, and J. E.-Y. Lee, "AlN-on-Si Square Diaphragm Piezoelectric Micromachined Ultrasonic Transducer with Extended Range of Detection," *Proceedings*, vol. 2, no. 13, Art. no. 13, 2018, doi: 10.3390/proceedings2130913.



www.manaraa.com

[55] Y. Lu *et al.*, "Broadband piezoelectric micromachined ultrasonic transducers based on dual resonance modes," in *2015 28th IEEE International Conference on Micro Electro Mechanical Systems (MEMS)*, Jan. 2015, pp. 146–149, doi: 10.1109/MEMSYS.2015.7050907.

[56] A. Guedes, S. Shelton, R. Przybyla, I. Izyumin, B. Boser, and D. A. Horsley, "Aluminum nitride pMUT based on a flexurally-suspended membrane," in *2011 16th International Solid-State Sensors, Actuators and Microsystems Conference*, Jun. 2011, pp. 2062–2065, doi: 10.1109/TRANSDUCERS.2011.5969223.

[57] U.-H. Lim, J.-H. Yoo, V. Kondalkar, and K. Lee, "Development of high frequency pMUT based on sputtered PZT," *J. Electr. Eng. Technol.*, vol. 13, pp. 2434–2440, Nov. 2018, doi: 10.5370/JEET.2018.13.6.2434.

[58] J. Jung, W. Lee, W. Kang, E. Shin, J. Ryu, and H. Choi, "Review of Piezoelectric Micromachined Ultrasonic Transducers and Their Applications," *J. Micromechanics Microengineering*, vol. 27, Aug. 2017, doi: 10.1088/1361-6439/aa851b.

[59] S. Sadeghpour, P. Pobedinskas, K. Haenen, and R. Puers, "A Piezoelectric Micromachined Ultrasound Transducers (pMUT) Array, for Wide Bandwidth Underwater Communication Applications," *Proceedings*, vol. 1, no. 4, Art. no. 4, 2017, doi: 10.3390/proceedings1040364.

[60] A. Safari and E. K. Akdogan, *Piezoelectric and Acoustic Materials for Transducer Applications*. Springer, 2008.

[61] J.-H. Mo, A. L. Robinson, D. W. Fitting, F. L. Terry, and P. L. Carson, "Micromachining for improvement of integrated ultrasonic transducer sensitivity," *IEEE Trans. Electron Devices*, vol. 37, no. 1, pp. 134–140, Jan. 1990, doi: 10.1109/16.43810.

[62] S. Shelton *et al.*, "CMOS-compatible AlN piezoelectric micromachined ultrasonic transducers," in *2009 IEEE International Ultrasonics Symposium*, Sep. 2009, pp. 402–405, doi: 10.1109/ULTSYM.2009.5441602.

[63] G. Perçin, A. Atalar, F. Levent Degertekin, and B. T. Khuri-Yakub, "Micromachined two-dimensional array piezoelectrically actuated transducers," *Appl. Phys. Lett.*, vol. 72, no. 11, pp. 1397–1399, Mar. 1998, doi: 10.1063/1.121067.



www.manaraa.com

[64] K. M. Smyth, “Piezoelectric micro-machined ultrasonic transducers for medical imaging,” Thesis, Massachusetts Institute of Technology, 2017.

[65] A. Arnau and D. Soares, “Fundamentals on Piezoelectricity,” in *Piezoelectric Transducers and Applications*, A. Arnau Vives, Ed. Berlin, Heidelberg: Springer, 2004, pp. 1–37.

[66] X. Liu, X. Chen, X. Le, Y. Wang, C. Wu, and J. Xie, “Reducing ring-down time of pMUTs with phase shift of driving waveform,” *Sens. Actuators Phys.*, vol. 281, pp. 100–107, Oct. 2018, doi: 10.1016/j.sna.2018.08.039.

[67] A. Dangi and R. Pratap, “System level modeling and design maps of PMUTs with residual stresses,” *Sens. Actuators Phys.*, vol. 262, pp. 18–28, Aug. 2017, doi: 10.1016/j.sna.2017.05.006.

[68] Y. Qiu *et al.*, “Piezoelectric Micromachined Ultrasound Transducer (PMUT) Arrays for Integrated Sensing, Actuation and Imaging,” *Sensors*, vol. 15, no. 4, Art. no. 4, Apr. 2015, doi: 10.3390/s150408020.

[69] M. W. Nygren, “Finite Element Modeling of Piezoelectric Ultrasonic Transducers,” p. 76.

[70] Z. Wei and L. K. Weavers, “Combining COMSOL modeling with acoustic pressure maps to design sono-reactors,” *Ultrason. Sonochem.*, vol. 31, pp. 490–498, Jul. 2016, doi: 10.1016/j.ultsonch.2016.01.036.

[71] A. Bayliss, M. Gunzburger, and E. Turkel, “Boundary Conditions for the Numerical Solution of Elliptic Equations in Exterior Regions,” *Siam J. Appl. Math. - SIAMAM*, vol. 42, Apr. 1982, doi: 10.1137/0142032.

[72] A. Cowen, G. Hames, K. Glukh, and B. Hardy, “PiezoMUMPs™ Design Handbook,” p. 28.

[73] H. Nazemi *et al.*, “Mass Sensors Based on Capacitive and Piezoelectric Micromachined Ultrasonic Transducers—CMUT and PMUT,” *Sensors*, vol. 20, no. 7, Art. no. 7, Jan. 2020, doi: 10.3390/s20072010.

[74] G. C. Bentel, L. B. Marks, P. H. Hardenbergh, and L. R. Prosnitz, “Variability of the depth of supraclavicular and axillary lymph nodes in patients with breast cancer: is a posterior axillary boost field necessary?,” *Int. J. Radiat. Oncol. Biol. Phys.*, vol. 47, no. 3, pp. 755–758, Jun. 2000, doi: 10.1016/s0360-3016(00)00485-5.



www.manaraa.com

[75] “Essentials of ultrasound physics / James A. Zagzebski. - Version details - Trove.” https://trove.nla.gov.au/work/16111527?q&versionId=18903562 (accessed Jun. 05, 2020).

[76] H. Kazari, M. Kabir, A. Mostavi, and D. Ozevin, “Multi-Frequency Piezoelectric Micromachined Ultrasonic Transducers,” *IEEE Sens. J.*, vol. 19, no. 23, pp. 11090–11099, Dec. 2019, doi: 10.1109/JSEN.2019.2935158.



www.manaraa.com

# VITA AUCTORIS

| | |
|---|---|
| NAME: | Jenitha Antony Balasingam |
| PLACE OF BIRTH: | Tamil Nadu, India |
| YEAR OF BIRTH: | 1995 |
| EDUCATION: | PSNA College of Engineering and Technology, B.Eng., Dindigul, Tamil Nadu, India. 2017 |
| | University of Windsor, M.A.Sc., Windsor, ON, 2020 |



www.manaraa.com